THEORETICAL CHEMISTRY INSTITUTE

THE UNIVERSITY OF WISCONSIN

DIATOMIC PREDISSOCIATION LINE WIDTHS

M. S. Child

WIS-TCI-416

30 March 1973

MADISON, WISCONSIN

ERRATA

Page	Position	Error	Correction
10	line 1	ang F(E)	arg F(E)
18	eqn (2.64)	$h\omega^*$	$\not{h}\omega^*$
20	line 15	table (2.41)	table 2.1
25	eqn (2.83) and line 20	h	$\not{h}$
50	lines 19, 21, 22	h	$\not{h}$
51	line 12	h	$\not{h}$
52	line 16	P_{vJ}	$\tilde{P}_{vJ}$
52	line 20	non-adiabatic	non-diabatic
56	eqn (3.83)	$h\bar{\omega}_{vo}$	$\not{h}\bar{\omega}_{vo}$
61	line 10	Bernstein [1966]	Bernstein [2]
68	line 7	[6]	[16]
68	line 10	[10]	[20]
72	Note (a)	[6]	[16]
72	Note (b)	[11]	[21]
72	Note (c)	[20]	[29]
75	Note (a)	LeRoy [40]	LeRoy [50]
75	Note (b)	[10]	[20]

Note: The quantity m is the reduced mass of the diatomic, more usually denoted μ .

DIATOMIC PREDISSOCIATION LINE WIDTHS *

M. S. Child†

Theoretical Chemistry Institute

University of Wisconsin

Madison, Wisconsin 53706 U.S.A.

Prepared for a Specialist Periodical Report of the Chemical Society (London) on Electronic Spectroscopy, edited by R. F. Barrow.

---

* This research was supported by the National Aeronautics and Space Administration Grant NGL 50-002-001.

† Present address: Theoretical Chemistry Department, 1 South Parks Road, Oxford, United Kingdom.

I. INTRODUCTION

The past five years have seen a revival of theoretical interest in predissociation phenomena, coupled with increasing sophistication in experimental technique [1] and a continuing search for related resonance effects in the molecular scattering field [2-5]. Given the established characterisations of predissociation types [6-7] and selection rules [8-9], and the accepted value of predissociation measurements in locating the dissociation limit [6,10], the object of recent theoretical work has been to underline further information available from individual line width (or lifetime) measurements. This information relates primarily to the forms of the relevant potential energy curves.

The purpose of this review is to summarise our present understanding of predissociation by rotation (type III [6]) and by curve crossing (type I [6]) in diatomic molecules. The material therefore falls into two parts, each of which includes a formal quantum mechanical introduction, which may also serve to emphasise the connection between spectroscopic measurements and molecular scattering data. Subsequent sections cover the available computational and analytical techniques, followed by a detailed summary of conclusions. An attempt has been made to include all line width or lifetime calculations for specific systems published before going to press (May 1973).

The first general conclusion is that the pattern of predissociation line widths provides a highly sensitive yardstick for the determination of unknown potential curves. Secondly, the computation of such a pattern for given potential curves is now a matter of routine, unless

the predissociation happens to occur from an upper adiabatic (avoided curve-crossing) potential curve. As an alternative to exact numerical computation one may expect to apply available relatively rapid analytical (semi-classical) estimates within an accuracy of 10%. These analytical formulae also to provide physical insight into the details of the predissociation pattern, to the extent that a direct inversion procedure has been developed for determination of the repulsive potential curves responsible for type I predissociations.

II. PREDISSOCIATION BY ROTATION

The relation between predissociation by rotation [6] and the shape or orbiting resonances of collision theory [2-5, 11] is by now well established. Both are due to the existence of a quasi-bound state separated from the continuum by a potential barrier, as depicted in figure 2.1, but the two types of experiment are, in fact, complementary since the scattering resonances most readily detected experimentally correspond to lines which would appear indiscernibly diffuse in the spectrum.

Much of the relevant theory is to be found either in the scattering literature, or at least couched in the language of scattering theory. Advances have been made by both computational [14-21] and semi-classical methods [13, 12-32]. Some computational workers have used the resonant jump in the scattering phase shift [14-17], or the closely associated peak in the collision delay time (see below) [20, 33-35] to determine the positions and energy widths of the quasi-bound

states. Others have pointed to the spectroscopically important peak in the relative amplitude of the wavefunction inside and outside the barrier region [14, 18-20]; however the intimate connection [12] between this characteristic and the behaviour of the phase shift has received relatively little emphasis in the molecular literature. Again in the semi-classical field attention has concentrated on the behaviour of the phase shift [24-27], or equivalently (see below) on the location of complex energy poles in the scattering matrix [28-30], but the behaviour of the amplitude ratio has been largely ignored.

Our first purpose will therefore be to demonstrate the necessary connection between resonant characteristics of the phase shift, $\eta(E)$, the collision delay time $\tau_d(E)$ and the amplitude ration, $A(E)$. This general discussion will involve the introduction of complex energy levels

$$E = E_n - i\Gamma_n/2 \ , \ \Gamma_n > 0 \qquad (2.1)$$

and lead to Breit-Wigner parameterisations of $\eta(E)$, $\tau_d(E)$, and $A(E)$. We shall then specialise to a semi-classical (JWKB) description in order to relate the reasonance positions, E_n, and widths, Γ_n, to the form of the potential function. Finally, the practical applications of the theory will be discussed.

§ 2.1 Resonance characteristics

Given that the quasi-bound state with angular momentum J, supported by a potential, $V(r)$, lies in the continuum it is convenient to take the energy zero at the dissociation limit, $V(\infty) = 0$, and to

define

$$k^2 = 2mE/\hbar^2$$

$$U(r) = 2mV(r)/\hbar^2 \ . \qquad (2.2)$$

The wavefunction must then satisfy

$$\left[\frac{d^2}{dr^2} + k^2 - U(r) - \frac{J(J+1)}{r^2} \right] \chi_{EJ}(r) = 0 \ , \qquad (2.3)$$

subject to the boundary condition $\chi_{EJ}(0) = 0$. The most convenient normalisation is to a delta function of energy [36] ;

$$\int_0^\infty \chi_{EJ}(r)\ \chi_{E'J}(r)dr = \delta(E - E') \ . \qquad (2.4)$$

This fixes the asymptotic amplitude of the wavefunction as,

$$\chi_{E,J}(r) \overset{r \to \infty}{\sim} \left[\frac{2m}{\pi\hbar^2 k} \right]^{1/2} \sin[kr - J\pi/2 + \eta_J(E)] \ , \qquad (2.5)$$

where $\eta_J(E)$ is the phase shift, the term $-J\pi/2$ being included in (2.5) so that $\eta_J(E) = 0$ in the absence of any distortion potential ($V(r) = 0$) . Closely associated with $\eta_J(E)$ is the collision delay time function [33-35]

$$\tau_d(E,J) = 2\hbar \frac{\partial \eta_J}{\partial E} \ , \qquad (2.6)$$

the resonance behaviour of which is more conveniently characterised than that of the phase shift [20].

The significance of the energy normalisation given by (2.4), is that it ensures unit density of states [37]. Hence the differential

oscillator strength for aspectroscopic transition from a bound level $\psi_b(r)$ of some other electronic states varies as

$$\nu \left| \int_0^\infty \chi_b(r) \, \underset{\sim}{M}(r) \, \chi_{E,J}(r) dr \right|^2 , \tag{2.7}$$

where $\underset{\sim}{M}(r)$ denotes the electronic transition moment. Thus, with the external amplitude fixed by (2.5), a peak in the internal to external amplitude ratio leads to strongly enhanced overlap with $\psi_b(r)$, and hence to a peak in the spectrum.

The necessary connection between the behaviour of this amplitude ratio and that of the phase shift is however most readily demonstrated by the introduction of a generalised solution $\psi_{kJ}(r)$ of (2.3), renormalised at the origin such that [12]

$$\lim_{r \to 0} r^{-J-1} \chi_{kJ}(r) = 1 , \tag{2.8}$$

and capable of extension to complex values of k ,

$$k = k' + ik'' , \tag{2.9}$$

and hence according to (2.2) to the complex energy levels given by (2.1), with

$$\begin{aligned} E_n &= (k_n'^2 - k_n''^2)\hbar^2/2m \\ \Gamma_n &= -2ik_n'k_n''\hbar^2/m . \end{aligned} \tag{2.10}$$

It may be shown [12] that this generalised solution may be expressed in the asymptotic region, $r \to \infty$, in terms of two Jost functions $f_J(\pm k)$,

$$\chi_{kJ}(r) \overset{r \to \infty}{\sim} \frac{1}{2i} [f_J(k)e^{ikr} - f_J(-k)e^{-ikr}] , \qquad (2.11)$$

where for complex k

$$f_J(-k) = [f_J(k^*)]^* , \qquad (2.12)$$

and $f_J(k)$ is analytic in k for $\mathrm{Im}\, k < 0$. It follows that for real k (and hence real E).

$$\chi_{kJ}(r) \overset{r \to \infty}{\sim} |f_J(k)| \sin(kr - J\pi/2 + \eta_J(E)] , \qquad (2.13)$$

where

$$\eta_J(E) = \arg f_J(k) + J\pi/2 , \qquad (2.14)$$

in agreement, apart from a change in normalisation with equation (2.5). This shows that both the amplitude ratio (which varies by virtue of the new normalisation condition (2.8), as $|f_J(k)|^{-1}$) and the phase shift depend on the behaviour of the function $f_J(k)$.

Particular attention attaches to complex roots of the $f_J(\pm k)$, of which two types may be recognised. The simplest are zeros of $f_J(k)$ on the negative imaginary axis, $k = -i\gamma_{vJ}$ say, so that according to (2.8)

$$\chi_{kJ}(r) \overset{r \to \infty}{\sim} A\, e^{-\gamma_{vJ} r} . \qquad (2.15)$$

These therefore correspond to the bound states with real negative energies $E_{vJ} = -\gamma_{vJ}^2 \hbar^2/2m$. The quasi-bound states on the other hand are associated with roots of $f_J(-k)$, given by (2.9) with $k' > 0$,

$k'' < 0$. Hence Γ_n given by (2.10) is positive. For roots of this type, $\Psi_{kJ}(r)$ has purely outgoing characteristics

$$\Psi_{kJ}(r) \overset{r \to \infty}{\sim} \frac{1}{2i} f_J(k) e^{ikr} , \tag{2.16}$$

and as might be expected for a quasi-bound state, the imaginary component in the energy given by (2.1) ensures an exponential decrease in the time evolution factor

$$\left| \exp(-iEt/\hbar) \right|^2 = \exp(-\Gamma_n t/\hbar) , \tag{2.17}$$

with time constant

$$\tau_n = \hbar/\Gamma_n . \tag{2.18}$$

Complex energy (and hence nonphysical) solutions of this type are termed Siegert [38] states, while the energies themselves are termed poles in the S matrix, because with the elements of S defined by the ratios of the outgoing to the incoming amplitudes of the wavefunction,

$$S_J = f_J(k)/f_J(-k) , \tag{2.19}$$

in the present single channel problem. Hence, S_J has a pole at every zero of $f_J(-k)$.

A linear expansion in the neighbourhood of such a pole,

$$f_J(k) = [f_J(-k)]^* = F(E)(E - E_n - i\Gamma_n/2) , \tag{2.20}$$

where $F(E)$ may vary slowly with E may now be used to demonstrate the characteristic resonance behaviour in the physical (real energy)

solutions of (2.3). Clearly according to (2.14) and (2.20), with A(E,J) used to denote the amplitude ratio

$$|A(E,J)|^2 \propto |F(E)|^{-2}[(E - E_n)^2 + \Gamma_n^2/4]^{-1} \qquad (2.21)$$

$$\eta_J(E) = \eta_J^o(E) + \arctan[\Gamma_n/2(E_n - E)] , \qquad (2.22)$$

where

$$\eta_J^o(E) = \arg F(E) + J\pi/2 , \qquad (2.23)$$

while the collision delay time defined by (2.6) becomes

$$\tau_d(E,J) = 2\hbar \frac{\partial \eta_J^o}{\partial E} + \frac{\Gamma_n \hbar}{(E - E_n)^2 + \Gamma_n^2/4} . \qquad (2.24)$$

These are the standard Breit-Wigner parametrisations of A(E,J) , $\eta_J(E)$ and $\tau_d(E,J)$.

Clearly, if Γ_n is sufficiently small that variations in F(E) may be ignored over the resonance region, both the spectroscopic line shape and the collision delay time functions follow the same Lorentzian form. The line width parameter Γ_n may therefore be taken as the full width at half height of either function. Γ_n may also be deduced from the maximum resonance increment, $4\hbar/\Gamma_n$, in the time delay function, or in a purely analytical treatment (see below) from the imaginary part of the pole in the S matrix.

Possible distortions in the line shape and changes in the peak position as the line width increases have recently been noted [20]. Since such distortions to A(E,J) and $\tau_d(E,J)$ depend on $|F(E)|$

and ang F(E) respectively, they may be expected to differ in kind. Hence in any comparison with experiment A(E,J) must be employed in spectroscopic, and $\tau_d(E,J)$ (or $\eta_J(E)$) in scattering applications.

These general considerations therefore underline the intimate connection between the resonance behaviour of $\eta_J(E)$, $\tau_d(E,J)$ and A(E,J) , and indicate the origin of the Breit-Wigner parameterisations given by (2.21)-(2.24) in the sharp resonance limit. The next step is to relate the resonance positions E_n and widths Γ_n to the form of the potential function V(r) .

§2.2 Semi-classical theory

The semi-classical (JWKB) method of solution of equation (2.3) relies on establishing connections between solutions of the form [39, 42]

$$\chi_{EJ}(r) = [k_J(r)]^{-1/2}\left[X' e^{i\int_x^r k_J(r)dr} + X'' e^{-i\int_x^r k_J(r)dr}\right] , \tag{2.25}$$

where [40]

$$k_J^2(r) = k^2 - U(r) - (J + \tfrac{1}{2})^2/r^2 , \tag{2.26}$$

which are valid in the regions $a << r << b$, $r >> c$ in figure 2.2, where

$$\frac{d}{dr}\left(\frac{1}{k_J(r)}\right) << 1 . \tag{2.27}$$

Such connections are based on more accurate model solutions of (2.3) in the non-classical regions around the turning points a, b, and c where $k_J(r) = 0$.

Changes in $\chi_{EJ}(r)$ will be followed by setting (X', X'') in (2.25) equal to (A', A''), (B', B'') or (C', C'') according to the choice of phase reference point x as a, b, or c ; single and double primes are used to denote outgoing and incoming motion respectively, as illustrated in figure 2.2. This means since the same function may be referred either to a or to b in the region a << r << b that

$$\begin{pmatrix} B' \\ \\ B'' \end{pmatrix} = \begin{pmatrix} e^{i\alpha_J^o} & 0 \\ \\ 0 & e^{-i\alpha_J^o} \end{pmatrix} \begin{pmatrix} A' \\ \\ A'' \end{pmatrix} , \qquad (2.28)$$

where

$$\alpha_J^o = \int_a^b k_J(r)dr . \qquad (2.29)$$

The significance of the superscript zero will become apparent later.

The correct behaviour of the wavefunction at an isolated left-hand turning point, a , now requires that $\psi_{EJ}(r)$ should behave as the asymptotic form of an Airy function [41], which is the exact solution of (2.3) for a linear approximation to the potential, decreasing exponentially into the non-classical region r < a . The appropriate form is [39, 42]

$$\chi_{EJ}(r) = A[k_J(r)]^{-1/2} \sin(\int_a^r k_J(r)dr + \pi/4) . \qquad (2.30)$$

Hence by comparison with (2.25) (with (A', A'') in place of (X', X'')),

$$A' = \frac{1}{2} Ae^{-i\pi/4} , \quad A'' = \frac{1}{2} Ae^{i\pi/4} . \qquad (2.31)$$

Equally, at energies below the dissociation limit for which $\psi_{EJ}(r)$ must decrease exponentially for $r > b$, it may be shown [42] that

$$\chi_{EJ}(r) = B[k_J(r)]^{-1/2} \sin(\int_r^b k_J(r)dr + \pi/4) , \qquad (2.32)$$

so that

$$B' = \frac{1}{2} Be^{i\pi/4} , \quad B'' = \frac{1}{2} Be^{-i\pi/4} . \qquad (2.33)$$

Consistency between (2.28), (2.31) and (2.33) requires that the energy shall be chosen to satisfy the Bohr quantisation condition

$$\alpha_J^o = \int_a^b k_J(r)dr = (n + \frac{1}{2})\pi . \qquad (2.34)$$

for a bound state. A semi-classical normalisation of the wavefunction [42] then yields values for A and B in (2.30) and (2.32),

$$A = (-1)^n B = \left[\frac{2m\hbar\bar{\omega}}{\pi\hbar^2}\right]^{1/2} , \qquad (2.35)$$

where $\hbar\bar{\omega}$ is the local energy level spacing, given by the quadrature

$$\hbar\bar{\omega} = \frac{\partial E}{\partial n} = \frac{\pi\hbar^2}{m} [\int_a^b k_J^{-1}(r)dr]^{-1} . \qquad (2.36)$$

Analysis of the quasi-bound states requires a proper treatment of the barrier region, in place of a simple boundary condition at b. Different models for the barrier yield different relations between (B', B'') and (C', C'') in figure 2.2 [22-30], but any connection formula is subject to the equations of flux conservation

$$|C'|^2 - |C''|^2 = |B'|^2 - |B''|^2 , \qquad (2.37)$$

and of symmetry under time reversal, so that the substitutions

$$(C', C'') \rightarrow (C''^*, C'^*) \quad \text{imply} \quad (B', B'') \rightarrow (B''^*, B'^*) \; . \tag{2.38}$$

Hence we may express the general connection in the form

$$\begin{pmatrix} C' \\ C'' \end{pmatrix} = \begin{pmatrix} \cosh\tilde{\gamma}\, e^{-i\tilde{\phi}} & -i \sinh\tilde{\gamma}\, e^{i\tilde{\theta}} \\ i \sinh\tilde{\gamma}\, e^{-i\tilde{\theta}} & \cosh\tilde{\gamma}\, e^{i\tilde{\phi}} \end{pmatrix} \begin{pmatrix} B' \\ B'' \end{pmatrix} , \tag{2.39}$$

and give specific expressions for the parameters $\tilde{\gamma}$, $\tilde{\theta}$ and $\tilde{\phi}$ for different barrier models in equations (2.59)-(2.76) below. Solution of (2.39) when $B' = 1$, $C'' = 0$ gives the following expressions for the barrier transmission and reflection probabilities

$$\begin{aligned} T &= |C'|^2 = \operatorname{sech}^2\tilde{\gamma} \\ R &= |B''|^2 = \tanh^2\tilde{\gamma} \; . \end{aligned} \tag{2.40}$$

It now remains merely to combine equations (2.28), (2.31) and (2.39) in order both to determine the phase shift and to express the external amplitudes (C', C'') in terms of the internal coefficient A ;

$$\begin{pmatrix} C' \\ C'' \end{pmatrix} = \begin{pmatrix} \cosh\tilde{\gamma}\, e^{-i\tilde{\phi}} & -i \sinh\tilde{\gamma}\, e^{i\tilde{\theta}} \\ i \sinh\tilde{\gamma}\, e^{-i\tilde{\theta}} & \cosh\tilde{\gamma}\, e^{i\tilde{\phi}} \end{pmatrix} \begin{pmatrix} e^{i\alpha_J^o} & 0 \\ 0 & e^{-i\alpha_J^o} \end{pmatrix} \begin{pmatrix} \frac{1}{2} A\, e^{-i\pi/4} \\ \frac{1}{2} A\, e^{i\pi/4} \end{pmatrix}$$

$$= \frac{1}{2} A \begin{pmatrix} [e^{\tilde{\gamma}} \cos \alpha_J + i\, e^{-\tilde{\gamma}} \sin \alpha_J]\, e^{(i/2)(\tilde{\theta} - \tilde{\phi} - \pi/2)} \\ [e^{\tilde{\gamma}} \cos \alpha_J - i\, e^{-\tilde{\gamma}} \sin \alpha_J]\, e^{-(i/2)(\tilde{\theta} - \tilde{\phi} - \pi/2)} \end{pmatrix}$$

$$= \frac{1}{2} A \, (\cosh 2\tilde{\gamma} + \sinh 2\tilde{\gamma} \cos 2\alpha_J) \begin{pmatrix} e^{i\delta} \\ e^{-i\delta} \end{pmatrix} , \qquad (2.41)$$

where

$$\alpha_J = \alpha_J^o - \frac{1}{2} (\tilde{\phi} + \tilde{\theta})$$

$$\delta = \arctan(e^{-2\tilde{\gamma}} \tan \alpha) + \frac{1}{2} (\tilde{\theta} - \tilde{\phi}) - \pi/4 . \qquad (2.42)$$

This means that, with $|C'|$ chosen to satisfy the asymptotic normalisation given by (2.5)

$$\psi_{EJ}(r) \underset{\sim}{\overset{r \to \infty}{}} \left[\frac{2m}{\pi\hbar^2 k}\right]^{1/2} \sin[kr - J\pi/2 + \eta_J^o(E) + \eta_J^{(res)}(E)] , \qquad (2.43)$$

where

$$\eta_J^o(E) = \lim_{r \to \infty} \{\int_c^r k(r)dr - kr + (J + \tfrac{1}{2})\pi/2 + \tfrac{1}{2} (\tilde{\theta} - \tilde{\phi})\} \qquad (2.44)$$

$$\eta_J^{(res)}(E) = \arctan(e^{-2\tilde{\gamma}} \tan \alpha) , \qquad (2.45)$$

while in the internal region, $a << r << b$,

$$\chi_{EJ}(r) = [\cosh 2\tilde{\gamma} + \sinh 2\tilde{\gamma} \cos 2\alpha]^{-1/2} \left[\frac{2m}{\pi\hbar^2 k(r)}\right]^{1/2} \sin(\int_a^r k(r)dr + \pi/4) . \qquad (2.46)$$

This differs from the bound state solution given by (2.30) and (2.35) by the factor

$$A(E,J) = [\hbar\bar{\omega}(\cosh 2\tilde{\gamma} + \sinh 2\tilde{\gamma} \cos 2\alpha_J)]^{-1/2} . \qquad (2.47)$$

Hence $|A(E,J)|^2$ governs the spectroscopic line shape.

Clearly, at least for large $\tilde{\gamma}$ when according to (2.40) the barrier transmission probability is low, resonances in $\eta_J(E)$ and $A_J(E)$ occur at energies E_{nJ} such that

$$\alpha_J = \int_a^b k_J(r)dr - \frac{1}{2}(\tilde{\theta} + \tilde{\phi}) = (n + \frac{1}{2})\pi . \qquad (2.48)$$

This may be regarded as the quantisation condition (2.34) for a bound level subject to a small (see below) level shift due to the phase terms $\frac{1}{2}(\tilde{\theta} + \tilde{\phi})$; as a rough estimate based on a linear expansion for α_J^o and neglect of any energy variation in $(\tilde{\theta} + \tilde{\phi})$,

$$\Delta E_{nJ} = E_{nJ} - E_{nJ}^o \simeq (\tilde{\theta}_{nJ} + \tilde{\phi}_{nJ})\hbar\bar{\omega}/2\pi , \qquad (2.49)$$

where E_{nJ}^o is the unperturbed level given by (2.34) and $\hbar\bar{\omega}$ is defined by (2.36). The subscripts imply that $\tilde{\theta}$ and $\tilde{\phi}$ are evaluated at the resonance point. E_{nJ} may also be obtained directly (and more accurately) from (2.48).

It may be seen with the help of (2.45) and (2.47), to the extent that energy variations in $\tilde{\gamma}$ are unimportant over the resonance region, first that the resonance part of collision delay time $\tau_d(E)$ and the line shape $|A(E,J)|^2$ have the same functionality

$$\tau_d^{res}(E,J) = 2\hbar \frac{\partial \eta^{(res)}}{\partial E} = 2\pi\hbar |A(E,J)|^2$$

$$= (2\pi/\bar{\omega})[\cosh 2\tilde{\gamma}_{nJ} + \sinh 2\tilde{\gamma}_{nJ} \cos 2\alpha_J]^{-1} , \tag{2.50}$$

and secondly that the total integrated intensity from a single line is equal to unity

$$\int_{E_{nJ}-\frac{1}{2}\hbar\bar{\omega}}^{E_{nJ}+\frac{1}{2}\hbar\bar{\omega}} |A(E,J)|^2 dE \simeq \frac{1}{h\bar{\omega}} \left(\frac{\partial E}{\partial \alpha_J}\right) \int_{n\pi}^{(n+1)\pi} \frac{d\alpha_J}{\cosh 2\tilde{\gamma}_{nJ} + \sinh 2\tilde{\gamma}_{nJ} \cos 2\alpha_J} = 1 . \tag{2.51}$$

This analysis therefore adds a further link to the theory of intensities in discrete and continuous spectra [43-44] by including the quasi-bound states.

The above general expressions are readily reduced to Breit-Wigner form over the sharp resonance region $(e^{2\tilde{\gamma}_{nJ}} >> 1)$, by the linear expansion

$$\alpha_J \simeq (n + \frac{1}{2})\pi + \left(\frac{\partial \alpha_J}{\partial E}\right)(E - E_{nJ})$$

$$\simeq (n + \frac{1}{2})\pi + \frac{\pi}{h\bar{\omega}} (E - E_{nJ}) , \tag{2.52}$$

with the results

$$\eta_J^{(res)}(E) = \arctan[\Gamma_{nJ}/2(E_{nJ} - E)] \tag{2.53}$$

$$\tau_d^{(res)}(E,J) = 2\pi\hbar |A(E,J)|^2 = \frac{\Gamma_{nJ}\hbar}{\frac{1}{4}\Gamma_{nJ}^2 + (E - E_{nJ})^2} , \tag{2.54}$$

where

$$\Gamma_{nJ} = (2\hbar\bar{\omega}/\pi)e^{-2\tilde{\gamma}_{nJ}} \tag{2.55}$$

Connor [28] and Dickinson [29] would obtain the same result directly from (2.41) by applying the outgoing boundary condition

$$C'' = e^{\tilde{\gamma}}\cos\alpha_J - ie^{-\tilde{\gamma}}\sin\alpha_J = 0 , \tag{2.56}$$

and the linear expansion (2.52), to obtain the complex energy of the Siegert state,

$$E = E_{nJ} - \frac{i}{2}(2\hbar\bar{\omega}/\pi)e^{-2\tilde{\gamma}_{nJ}} . \tag{2.57}$$

Note that in this sharp resonance limit, $e^{-2\tilde{\gamma}_{nJ}} << 1$, Γ_{nJ} is directly related to the barrier transmission probability given (2.40) in the semi-classical form [3].

$$\Gamma_{nJ} = T\hbar/t_{vib} , \tag{2.58}$$

where $t_{vib} = 2\pi/\bar{\omega}$.

It remains to determine the parameters $\tilde{\gamma}$, $\tilde{\theta}$ and $\tilde{\phi}$ in (2.39), for different barrier models. The simplest theory employs independent semi-classical connection formulae at the turning points b and c [22-23] with the results

$$\tilde{\gamma}_{nJ} = \int_b^c |k_{nJ}(r)|dr + \ell n2 \tag{2.59}$$

$$\tilde{\theta}_{nJ} = \tilde{\phi}_{nJ} = 0 , \tag{2.60}$$

where the subscript on $k_{nJ}(r)$ implies that the energy is chosen to satisfy (2.48). This may be termed the simple semi-classical estimate. The first improvements [24, 26, 28] employ a quadratic approximation at the barrier maximum

$$V_J(r) = V_J^{max} - \frac{1}{2}\mathcal{K}(r - r_{max})^2 , \tag{2.61}$$

to obtain

$$\tilde{\gamma}_{nJ} = \cosh^{-1}[1 + e^{-2\pi\varepsilon}]^{1/2} , \tag{2.62}$$

$$\tilde{\phi}_{nJ} = \phi(\varepsilon) = \Gamma(\tfrac{1}{2} + i\varepsilon) - \varepsilon \ell n|\varepsilon| + \varepsilon , \tag{2.63}$$

$$\tilde{\theta}_{nJ} = 0 ,$$

where

$$\varepsilon = (E_{nJ} - V_J^{max})/\hbar\omega^*$$

$$\omega^* = (\mathcal{K}/m)^{1/2} \tag{2.64}$$

Methods employed by other workers give the same form for $\tilde{\gamma}_{nJ}$ but either a different phase correction [13], or an undetermined phase connection [25, 27, 30]. Values of the function $\phi(\varepsilon)$ which determines the level shift in (2.49) and some limiting properties [13, 26, 45] are given in table 2.1. A function of this form also plays an important part in scattering theory by removing a classical singularity in the deflection function [13]. Equations (2.62)-(2.64) define what we shall term the JWKB quadratic approximation. Miller and Good [46] have shown how this quadratic approximation may be replaced by a more general

association between the physical barrier and the quadratic form (2.61), the association being defined by the identity

$$\varepsilon = -\frac{1}{\pi}\int_b^c |k_{nJ}(r)|\,dr \ , \qquad (2.65)$$

which takes place of (2.64). Our name for this improvement is the associated quadratic approximation. First suggested without proof by Connor [45], it reduces to (2.64) in the quadratic approximation and causes the expression (2.62) for $\tilde{\gamma}_{nJ}$ to go over to the simple semi-classical form (2.59) when $e^{-2\pi\varepsilon} >> 1$ (recall that $\varepsilon < 0$ for energies below the barrier maximum). Since however [13,27,45]

$$\phi(\varepsilon) \sim \frac{1}{24}\varepsilon^{-1} + \frac{7}{2880}\varepsilon^{-3} \quad \text{for } \varepsilon > 1 \ , \qquad (2.66)$$

the level shifts predicted by equations (2.49) and (2.63) (but not covered by the simple semi-classical theory) depend inversely, rather than exponentially, on ε. Hence the leve shift may be orders of magnitude larger than the line width in the sharp resonance region.

Dickinson [29] and Soop [47] have taken the association method one stage further in order to obtain a two parameter description. Dickinson [29] relies on an association between $k_{nJ}^2(r)$ and the inverted Morse form

$$t^2\{q^2 - [2e^{-s} - e^{-2s}]\} \ , \qquad (2.67)$$

where q^2 is the ratio of the available energy to the barrier height (measured from the dissociation limit) and t is defined by the equation

$$\pi t(1 - q) = \int_b^c |k_{nJ}(r)|\,dr \ , \tag{2.68}$$

where, as in (2.65), $k_{nJ}(r)$ contains the true potential function. The expressions (2.62)-(2.65) are then replaced in the present notation, by

$$\tilde{\gamma}_{nJ} = \sinh^{-1}[e^{-\pi\varepsilon_-} \cosh \pi\varepsilon_+/\sinh 2\pi qt] \tag{2.69}$$

$$\tilde{\phi}_{nJ} = \chi(2qt) - \phi(\varepsilon_-) \tag{2.70}$$

$$\tilde{\theta}_{nJ} = \chi(2qt) - \phi(\varepsilon_+) \tag{2.71}$$

where

$$\varepsilon_\pm = t(1 \pm q) \tag{2.72}$$

$$\chi(y) = \arg\Gamma(iy) - y\ell n|y| + y + \pi/4 = \chi(2y) - \phi(y) \tag{2.73}$$

and $\phi(\varepsilon)$ is defined by (2.63). This we shall term the associated Morse approximation. Note that ε_- is identical with $-\varepsilon$ defined by the quadratic association formula (2.65). Furthermore t is typically large unless the barrier is very low (t lies in the range 4-15 for J levels of the H_2 ground state considered in table (2.41)), and $\chi(y) \sim -1/12y$ for $y > 2$. Hence it may be verified that (2.69)-(2.72) reduce to (2.62)-(2.63) with t given by (2.65) except for very low barriers (low J values) or for (very sharp) levels close to the base of the barrier.

A final somewhat similar (associated sech^2) form may be obtained from the results of Soop [47] based on association between $k_{nJ}^2(r)$ and

$$t^2\{q^2 - \mathrm{sech}^2 s\} \ . \qquad (2.74)$$

The parameters q and t have the same definitions as those of Dickinson, but now

$$\begin{aligned} \tilde{\gamma}_{nJ} &= \sinh^{-1}\left\{\frac{\cosh[\pi(t^2 - \tfrac{1}{4})]}{\sinh \pi q t}\right\} \\ \tilde{\phi}_{nJ} &= 2\chi(qt) - \phi(\varepsilon'_-) + \phi(\varepsilon'_+) + \delta \\ \tilde{\theta}_{nJ} &= 0 \ , \end{aligned} \qquad (2.75)$$

where

$$\varepsilon'_\pm = (t^2 - \tfrac{1}{4})^{1/2} \pm qt$$

$$\delta = t\ell n\left|\frac{1+q}{1-q}\right| - (t^2 - \tfrac{1}{4})^{1/2}\ell n(\varepsilon'_+/\varepsilon'_-) - qt\ell n\left[\frac{\varepsilon'_+\varepsilon'_-}{(1-q^2)t^2}\right] . \qquad (2.76)$$

§ 2.3 Quasi-bound energy levels

Any attempt to calculate the width of a quasi-bound state requires prior knowledge of its position. Calculated level positions have been reported for the ground states the H_2 [14, 15, 17, 19, 20, 22, 23] HD and D_2 [20], OH [19] $^4HeH^+$, $^3HeH^+$, $^4HeD^+$, $^3HeH^+$ [5], and ArK and RbK [31] systems and for a standard model based on the Lennard-Jones potential [16, 21, 29].

The first calculations [14, 15, 17] employed the points of inflexion in the phase shift, $\eta_J(E)$, derived by numerical integration of (2.3), but this approach has been superceded by use of the time delay function,

$\tau_d(E,J)$ [20], after recognition that $\tau_d(E,J)$ may be derived from the same scattering solution, normalised in the form

$$\tilde{\chi}_{EJ}(r) \overset{r \to \infty}{\sim} (4m/\hbar k)^{1/2} \sin\{kr - J\pi/2 + \eta_J(E)\} , \qquad (2.78)$$

by the quadrature [35],

$$\tau_d(E,J) = \int_o^\infty (|\psi_{EJ}(r)|^2 - |\psi_{EJ}(\infty)|^2) dr + (m/\hbar k^2) \sin(2\eta_J(E) - J\pi) . \qquad (2.79)$$

Hence the resonance points, and particularly the level widths, may be obtained more conveniently from the maxima in $\tau_d(E,J)$. The positions of peaks in the amplitude ratio, $A(E,J)$, first demonstrated by Buckingham and Fox [14], have also been employed [18,20]. Results derived from $A(E,J)$ for the ground state of H_2 are found to agree within $0.1\ cm^{-1}$ with those derived from $\tau_d(E,J)$ [20] for the sharp resonances ($\Gamma < 5\ cm^{-1}$) but discrepancies, due to variation of the ambient phase shift $\eta_J^o(E)$ in (2.22), of the order of $1\text{-}6\ cm^{-1}$ are reported for the broad levels [18, 20] (see table 2.3). Resonance positions discussed below refer to the maxima in $A(E,J)$, as having the greatest spectroscopic significance.

A major problem encountered in these calculations is that in seeking the scattering solution (such that $\psi_{EJ}(0) = 0$) there is no efficient algorithm for converging on a resonance, a problem which becomes acute for very sharp resonances [20]; the method proposed by Johnson, Balint-Kusti and Levine [48] suffers from the same disadvantage. Bain and Bardsley [21] have therefore devised a different exact procedure

specifically for the treatment of sharp resonances. Two solutions of (2.3) are introduced, one of which, $f(r)$, is defined to have zero derivative at the origin and to behave as

$$f(r) \overset{r \to \infty}{\sim} \sin(kr + \delta) \tag{2.80}$$

at infinity. The second solution, $g(r)$, is chosen such that

$$g(r) \overset{r \to \infty}{\sim} \cos(kr + \delta) \tag{2.81}$$

and integrated back to the origin. The resonances are then shown to occur at energies for which $g(0) = 0$, and the level widths for rotationless states $(J = 0)$ to be given by an expression analogous to (2.79),

$$\Gamma_{nJ} = \frac{\hbar^2 k}{m} \lim_{R \to \infty} \{[\int_0^R (g^2(r) - f^2(r))dr - \frac{1}{2k} \sin(2kR + 2\delta)]^{-1}\} . \tag{2.82}$$

A similar more complicated expression is given for $J \neq 0$. A comparison between the level positions obtained for the Lennard-Jones model and those derived from the phase shift is given in table 2.2.

Other more approximate methods have also been suggested. One approach is to convert the problem into a bound state form by imposing a boundary condition either at the barrier maximum [19, 20], or at the outermost turning point [5, 20]. Studies on the H_2 ground state [20] (see table 2.3) favoured the requirement that the wavefunction should behave as an Airy function of the second type (increasing exponentially into the barrier region) at the outermost turning point; a similar suggestion [5] is that $\psi_{EJ}(r)$ should have the same logarithmic

derivative at this point as the irregular Bessel function $Y_{J+\frac{1}{2}}(kr)$ [41]. This approach still requires numerical solution of the Schrodinger equation. The semi-classical theory of § 2.2 shows that this may be replaced merely by two quadratures (over the potential well $a < r < b$, and the barrier $b < r < c$) at each point on a suitable energy grid. Dickinson [29] has applied the modified quantisation condition equation (2.4), with $(\tilde{\theta} + \tilde{\phi})$ given (2.63) and (2.65), to obtain level positions for the Lennard-Jones model in good agreement with the exact values (see table 2.2). It is interesting that almost equally good agreement may be achieved with a different phase correction by taking the JWKB theory to second order [16]. Bayliss [31] has also obtained good agreement with exact numerical results [49] for the heavier KAr and RbAr systems using this second (now very small) phase correction.

§ 2.4 Level widths

Given the resonance position, computation of the level width presents little difficulty. Values have been obtained from the slope of $\eta_J(E)$ [14, 15, 17], from the width and resonance value of $\tau_d(E,J)$ [20], from the width [18, 20] and the peak value [5] of the amplitude ratio A(E,J), from the special formula of Bain and Bardsley [21] and from the semi-classical equations (2.55) and (2.59)-(2.76) [29, 32]. Comparisons are given for the Lennard-Jones system [16, 21, 29] and for the ground state of H_2 [20] in tables 2.2 and 2.3 respectively. The most striking feature is the accuracy of the very rapid JWKB estimates. The values obtained by Dickinson [29] for the Lennard-Jones system in the associated Morse approximation (equations (2.55),

(2.68)-(2.72)) agree to within 10% with the exact values of Bain and Bardsley [21], and with the probably less accurate values derived from the slope of the phase shift by Bernstein et al. [16]. This agreement is possibly not surprising since these resonances are very sharp. Table 2.3 also shows close agreement between the exact line widths and the simplest semi-classical estimates (equation (2.59)) [20]; and this agreement may be improved for the broader levels ($\Gamma > 20$ cm^{-1}), with no more effort by use of the more refined associated parabolic equations (2.62) and (2.65) in place of (2.59). Thus the simple semi-classical estimate $\Gamma^{(0)}$ may be improved to a value $\Gamma^{(1)}$ by the algorithm

$$\Gamma^{(1)} = (2\hbar\bar{\omega}/\pi)e^{-2\tilde{\gamma}}$$

$$\tilde{\gamma} = \cosh^{-1}\{[1 + h\bar{\omega}/2\pi\Gamma^{(0)}]^{1/2}\} . \quad (2.83)$$

Values of $\hbar\bar{\omega}$, defined by (2.36), required for the computation of $\Gamma^{(0)}$ were not reported [20], but estimates may be obtained from the tables of accurate level positions given by LeRoy [50]. In fact quite rough estimates will suffice, since the level of agreement between $\Gamma^{(1)}$ and the exact values shown in table 2.4 ($|\Gamma^{(1)} - \Gamma_{exact}| <$ 0.5 cm^{-1} except for the two broadest levels, (v,J) = (0,38) and (8,21)) is unaffected by an increase in $h\bar{\omega}$ by 100 cm^{-1}. The final columns of table 2.4 also contain values of Dickinson's parameters q and t defined by (2.68), in order to demonstrate by the magnitude of t ($\pi t >> 1$) the essential equivalence between the associated quadratic and associated Morse approximations for the levels in question. Hence the associated quadratic approximation which requires the three quadratures

defined in (2.36), (2.42) and (2.65), may be taken to be the optimum semi-classical form for most purposes.

From an experimental viewpoint the most important theoretical conclusion is the very strong (exponential) energy dependence of the level width. Thus, as confirmed by experiment [51], a typical rotational progression for a hydride system will terminate in absorption in the form sharp, broad, very diffuse, followed by a complete loss of structure which may obscure the existence of one or possibly two quasi-bound ($E_{nJ} < V_J^{max}$) upper state levels. This must result in a discrepancy between the curve of limiting predissociation and the locus of the barrier maximum, V_J^{max}, which is estimated by LeRoy and Bernstein [20] to range from zero at $J = 0$ to as much as $1000\ cm^{-1}$ at $J = 38$ for the ground state of H_2. Hence although extrapolation of the limiting curve should yield the correct dissociation limit [6,10], deductions about the long range behaviour of the potential [52-54] must be treated with caution. Any attempt to extrapolate from observed data to the true locus of V_J^{max} requires an understanding of both the measurably sharp and the very broad levels discussed above.

§ 2.5 Summary and conclusions

The properties of non-physical Siegert states with complex energy levels, exponentially decreasing time evolution and purely outgoing characteristics have been used in 2.1 to unify the resonance behaviour of the phase shift the collision delay time and the spectroscopically observed internal to external amplitude ratio. The existence of such states also explains the Breit-Wigner parameterisations of $\eta_J(E)$, $\tau_d(E,J)$ and $A(E,J)$ (equations (2.21)-(2.24)).

A general semi-classical theory leads first in§2.2 to a quantisation condition (equation (2.48)) and to expressions for the levelshift, (2.49), and for the line width (2.55) in terms of three parameters $\tilde{\gamma}_{nJ}$, $\tilde{\theta}_{nJ}$ and $\tilde{\phi}_{nJ}$. Formulae for these parameters are then given for four different treatments of the barrier region, of which the associated quadratic model, equations (2.62), (2.63) and (2.65), appears to be the most generally applicable.

Different techniques for the location of quasi-bound states are discussed in§2.3. The most significant practical conclusion is that the (associated quadratic) semi-classical quantisation condition appears to be remarkably accurate.

Recent semi-classical formulae for the level width are also shown to achieve high accuracy even for very broad levels. Thus there would appear to be little necessity for exact numerical computations in this field. The existence of reliable analytical formulae may also be expected to lead to more accurate location of barrier maxima, in cases where the highest quasi-bound levels are indiscernably diffuse.

III. PREDISSOCIATION BY INTERNAL EXCITATION

Just as predissociation by rotation may be seen as another manifestation of a shape or orbiting resonance, so is predissociation by internal (electronic) excitation (Herzberg's type I [6]) associated with the Fano [69] or Feshbach [70] resonance phenomenon in scattering theory. The situation is complicated by the necessity to consider at least two electronic states. Physical mechanisms and selection rules

governing the necessary mixing of electronic states have been well characterised [8, 9] for many years. Our present interest is in the origin of the detailed dependence of the line width or lifetime pattern as a function of vibrational and rotational state. Recent work [56-68] has confirmed an early suggestion by Rice [55] that fluctuations in the line width, due to interference between the nuclear wavefunctions for the interacting state, provide a sensitive measure of forms of the relevant potential energy curves.

The subsequent theory is set in context by a short resumé of the Fano [69] theory of interaction between discrete levels and the continuum; alternative approaches have been suggested by Feshbach [70] and more recently by Van Santen [71]. We also include for the sake of completeness a brief account of possible electronic origins of the interaction term.

§ 3.1 The Fano lineshape

Fano [69] first considers the coupling between a single discrete level ϕ_n and a continuum of states ψ_E. Second order interaction between ϕ_n and other discrete states $\phi_{n'}$, are therefore neglected at this stage. The normalisations are chosen such that

$$\begin{aligned} (\phi_n|H|\phi_n) &= E_n \,, \\ (\psi_{E'}|H|\psi_{E''}) &= E'\delta(E'' - E') \\ (\psi_{E'}|H|\phi_n) &= (\phi_n|H|\psi_{E'})^* = V_{E'n} \,. \end{aligned} \tag{3.1}$$

This implies according to (2.5) that

$$\psi_{E'} \overset{r \to \infty}{\sim} \tilde{\psi}_{E'} \left[\frac{2m}{\pi\hbar^2 k'} \right]^{1/2} \sin[k'r + \delta(E')] \ , \qquad (3.2)$$

where $\tilde{\psi}_{E'}$ depends on the other (electronic and angular) coordinates of the system. Our purpose is to find an (energy-dependent) eigenfunction

$$\Psi_E = a(E)\phi_n + \int b(E,E')\psi_{E'}dE' \ , \qquad (3.3)$$

subject to the same asymptotic normalisation. The functions $a(E)$ and $b(E,E')$ will then determine the line shape.

It follows from (3.1) and (3.3) that at the energy eigenvalue E,

$$E_n a(E) + \int V_{nE'} b(E,E')dE' = Ea(E) \qquad (3.4)$$

$$V_{E'n} a(E) + E'b(E,E') = Eb(E,E') \ . \qquad (3.5)$$

$b(E,E')$ is now eliminated in favour of an admixture ratio $Z(E)$ which becomes the central quantity in the theory, by a rearrangement of (3.5) [36];

$$b(E,E') = \left[\frac{1}{E - E'} + Z(E)\delta(E - E') \right] V_{E'n} a(E) \ . \qquad (3.6)$$

At the same time the presence of the resulting pole due to the term $(E - E')^{-1}$ makes it necessary to specify how the integrations in (3.3) and (3.4) are to be carried out; otherwise $Z(E)$ is not uniquely defined. The most convenient choice is the Cauchy principal value [72], denoted by P below.

Hence on substitution for $b(E,E')$ in (3.4) and removal of the common factor $a(E)$

$$Z(E) = \frac{E - E_n - F(E)}{|V_{nE}|^2} , \tag{3.7}$$

where

$$F(E) = P\int_{-\infty}^{\infty} \frac{|V_{nE'}|^2 dE'}{E - E'} . \tag{3.8}$$

It remains to determine $a(E)$ by applying the asymptotic normalisation condition (3.2) to Ψ_E in (3.3). Equations (3.2), (3.3) and (3.6), together with the identity

$$\begin{aligned} P\int_{-\infty}^{\infty} \frac{\sin(k'r + \delta)}{(E - E')} dE' &= P\int_{-\infty}^{\infty} \left(\frac{2k'}{k + k'}\right) \frac{\sin[(k - k')r + kr + \delta]}{(k - k')} dk' \\ &= P\int_{-\infty}^{\infty} \left(\frac{2k'}{k + k'}\right) \cos(kr + \delta) \frac{\sin(k' - k)r}{(k - k')} dk' \\ &= -\pi \cos(kr + \delta) , \end{aligned} \tag{3.9}$$

imply that

$$\begin{aligned} \Psi_E \overset{r \to \infty}{\sim} \tilde{\psi}_E \left[\frac{2m}{\pi\hbar^2 k}\right]^{1/2} a(E)V_{En}\{-\pi \cos(kr + \delta) + Z(E)\sin(kr + \delta)\} \\ \sim \tilde{\psi}_E \left[\frac{2m}{\pi\hbar^2 k}\right]^{1/2} a(E)V_{En}[\pi^2 + Z^2(E)]^{1/2}\sin(kr + \delta + \delta^{(r)}) , \end{aligned} \tag{3.10}$$

where

$$\tan \delta^{(r)} = -(\pi/Z(E)) , \tag{3.11}$$

because $\phi_n \overset{r \to \infty}{\sim} 0$. Hence for the correct asymptotic behaviour

$$a(E) = V_{nE}^{-1} [\pi^2 + Z^2(E)]^{-1/2} . \tag{3.12}$$

This function, which represents the amplitude of the discrete component ϕ_n in the energy normalised solution (3.3), is the direct analogue of the amplitude ratio $A(E)$ of the previous section

With $Z(E)$ given by (3.7), equations (3.11) and (3.12) show that $\delta^{(r)}$ and $a(E)$ have the characteristic Breit-Wigner resonance behaviour, given by (2.21) and (2.22),

$$\delta^{(r)} = \arctan[\Gamma_n/2(E_n' - E)] , \tag{3.13}$$

$$|a(E)|^2 = \frac{1}{2\pi}\left[\frac{\Gamma_n}{(E - E_n')^2 + \frac{1}{4}\Gamma_n^2}\right] , \tag{3.14}$$

where

$$E_n' = E_n + F(E) \tag{3.15}$$

$$\Gamma_n = 2\pi|V_{nE}|^2 . \tag{3.16}$$

Furthermore by analogy with (2.51)

$$\int_{E_n'-\Gamma_n/2}^{E_n'+\Gamma_n/2} |a(E)|^2 dE = 1 . \tag{3.17}$$

Notice that the level width Γ_n depends, via V_{nE}, only on the resonance continuum state ψ_E, but that the levelshift function $F(E)$ appears in (3.9) as an integral over the full continuum. Both Γ_n and $F(E)$ are strictly energy dependent but they may be evaluated with sufficient accuracy at the resonance point E_n if the line width is small compared with the level spacing.

Finally Fano [69] obtains a compact expression for the spectroscopic transition moment by collecting the above results in the form

$$\Psi_E = \frac{1}{\pi V_{nE}} \Phi_n \sin \delta^{(r)} - \psi_E \cos \delta^{(r)} , \qquad (3.18)$$

where Φ_n represents the original discrete state ϕ_n modified by an admixture of continuum states,

$$\Phi_n = \Phi_n + P\int \frac{V_{nE'}\psi_{E'}}{E - E'} dE' . \qquad (3.19)$$

Hence the transition moment between Ψ_E and another state ϕ_o becomes

$$(\Psi_E|T|\phi_o) = \frac{1}{\pi V^*_{nE}} (\Phi_n|T|\phi_o) \sin \delta^{(r)} - (\psi_E|T|\phi_o) \cos \delta^{(r)} . \qquad (3.20)$$

The spectroscopic absorption line shape therefore differs according to the relative values of $(\Phi_n|T|\phi_o)$ and $(\psi_E|T|\phi_o)$. It takes the Lorentzian form

$$|(\Psi_E|T|\phi_o)|^2 = \frac{\Gamma_n}{2\pi[(E - E'_n)^2 + \Gamma_n^2/4]} |(\phi_n|T|\phi_o)|^2 , \qquad (3.21)$$

when transitions between ϕ_o and the continuum ψ_E are forbidden, but appears as a Lorentzian emmission line, against the continuum absorption, if $(\Phi_n|T|\phi_o) = 0$;

$$|(\Psi_E|T|\phi_o)|^2 = \left\{1 - \frac{\Gamma_n^2/4}{[(E - E'_n)^2 + \Gamma_n^2/4]}\right\} |(\psi_E|T|\phi_o)^2 . \qquad (3.22)$$

Interference between the two terms in (3.20), results in a distorted

line shape (see figure 3.1) characterised by Fano [69] in terms of the ratio

$$q = (\Phi_n|T|\phi_o)/\pi V^*_{nE}(\psi_E|T|\phi_o) \quad . \tag{3.23}$$

Herzberg and Jungen [73] have observed this characteristic Fano or Beutler [74] line shape in the pre-ionised Rydberg spectrum of H_2 .

Fano [69] also extends the argument to cover several discrete states ϕ_n interacting with one continuum ψ_E , and several continua $\psi_E^{(i)}$ interacting with one discrete state. The former naturally always applies in diatomic systems, but corrections to the one level analysis above become significant only when the line width given by (3.16) becomes comparable with the level spacing. The latter situation may arise in certain diatomic molecules, but it is of more general significance in the polyatomic case because each (vibrational-rotation) channel has an associated continuum of states [75].

The major correction to the theory in the many level, one continuum case is that the perturbed levels appear as the eigenvalues, E_ν , of a level shift matrix [69] with elements $E_n\delta_{nm} + F_{nm}(E)$, where

$$F_{nm}(E) = P\int \frac{V_{nE'}V_{E'm}dE'}{E - E'} \quad . \tag{3.24}$$

This leads to the introduction of transformed discrete state combinations

$$\phi_\nu = \sum_n c_{\nu n}\phi_n \tag{3.25}$$

where the $c_{\nu n}$ form the eigenvectors of the above matrix. The energy normalised solution Ψ_E finally appears in the form

$$\Psi_E = \cos\delta^{(r)}\{\sum_\nu \frac{V_{E\nu}}{E - E_\nu}\Phi_\nu - \psi_E\} , \qquad (3.26)$$

where

$$\tan\delta^{(r)} = \sum_\nu \frac{\pi|V_{E\nu}|^2}{E - E_\nu} \qquad (3.27)$$

$$\Phi_\nu = \phi_\nu + P\int \frac{V_{\nu E'}\psi_{E'}dE'}{E - E'} . \qquad (3.28)$$

The conditions for the validity of (3.15)-(3.18) are therefore first that $|F_{nm}(E)| \ll E_n - E_m$, so that

$$E_\nu \simeq E_n + F_{nn}(E) , \qquad (3.29)$$

and secondly than $|V_{En}| \ll E_\nu - E_{\nu'}$ in which case the sums in (3.27) and (3.28) may be approximated by a single term at each resonance, and the term $[\cos\delta^{(r)}V_{E\nu}/(E - E_\nu)]$ reduces to $(\sin\delta^{(r)}/\pi V_{nE})$ as in (3.18).

The results for the one discrete, several continua case may be summarised in the form [69]

$$\Psi_E = \frac{1}{\pi V_{nE}}\Phi_n \sin\delta^{(r)} - \sum_i \frac{V_{nE}^{(i)}}{V_{nE}}\psi_E^{(i)}\cos\delta^{(r)} , \qquad (3.30)$$

where

$$\Phi_n = \phi_n + \sum_i P\int \frac{V_{nE'}^{(i)}\psi_{E'}^{(i)}dE'}{E - E'} ,$$

$$V_{nE}^2 = \sum_i |V_{nE}^{(i)}|^2 , \qquad (3.31)$$

and $\delta^{(r)}$ is given by (3.13). Both the level shift $F(E)$, and the

line width Γ_n therefore appear, via V_{nE} in (3.25), as a simple sum of the previous single continuum formulae taken over the continua in question.

§ 3.2 The interaction term

The theory in the previous section is quite general. When specialised to a diatomic system the interaction term may be written

$$V_{nE'} = \int_0^\infty \chi_{2n}(r)\, H_{21}(r)\, \chi_{1E}(r)\, dr \,, \tag{3.32}$$

where

$$H_{21}(r) = \langle P_2 | H(\underset{\sim}{q},\underset{\sim}{r}) | P_1 \rangle \,. \tag{3.33}$$

Here n denotes a particular vibrational, total angular momentum level, $|P_1\rangle$ and $|P_2\rangle$ are used to designate appropriate electronic and rotational angular momentum states, and the integral in (3.33) is taken over the electronic coordinates $\underset{\sim}{q}$ and the angular coordinates of the nuclear position variable $\underset{\sim}{r}$. $\chi_{2n}(r)$ and $\chi_{1E}(r)$ are the corresponding vibrational and continuum wavefunctions, normalised to unity and to a delta function of energy respectively.

Predissociation may be induced by both internal (intramolecular) and external interactions. The important internal cases are covered by the selection rules and expressions for $H_{12}(r)$ given by Kronig [8]. These require in every case

$$\Delta J = 0 \quad , \quad + \leftrightarrow + \quad , \quad g \leftrightarrow u \quad , \tag{3.34}$$

but interactions governed by

$$\Delta\Lambda = 0,\pm 1 \qquad \text{in cases (a) and (b)}$$

$$\Delta\Omega = 0,\pm 1 \qquad \text{in case (c)} \tag{3.35}$$

are allowed. There is also a weak selection rule

$$\Delta S = 0 \qquad \text{in cases (a) and (b)}$$

which may be broken by spin-orbit coupling. An important observational distinction is made between homogeneous and heterogeneous interactions [76] for which $\Delta\Lambda = 0$ (or $\Delta\Omega = 0$ in case (c)) and $\Delta\Lambda = \pm 1$ (or $\Delta\Omega = \pm 1$) respectively, in that the latter (which arise from rotational-electronic coupling) yield an expression for $H_{12}(r)$ proportional to $[J(J+1) - \Lambda(\Lambda \pm 1)]^{1/2}$. A short table of expressions for $H_{12}(r)$ evaluated in the approximation of pure precession has been given by Czarny, Felenbok and Lefebvre-Brion [61].

Observed predissociations have also been attributed to the external interactions induced by magnetic fields [9, 77] and molecular collisions [80-82]. A condensed form of Van Vleck's theory [9] of magnetically induced predissociation has recently been given by Chapman and Bunker [79]. Qualitative aspects of the theory of pressure induced predissociation have been considered [81, 83] but a comprehensive theory remains to be developed.

§ 3.3 The Franck-Condon approximation

The existence of an intersection between the repulsive and bound state curves, $V_1(r)$ and $V_2(r)$ respectively, may be used to justify a significant simplification in equation (3.32), because the effective

integration region is known [84] to be localised at the crossing point, R; an analytical estimate obtained in §3.5 suggests an effective range between ± 0.05 Å and ± 0.20 Å in typical systems. Under these conditions it may be permissible to replace $H_{12}(r)$ by its value, H_{12}^{o}, at the crossing point, so that

$$\Gamma_n = 2\pi |V_{nE}|^2 = 2\pi |H_{12}^{o}|^2 \left| \int_0^\infty \chi_{2n}(r)\, \chi_{1E}(r) dr \right|^2 . \quad (3.36)$$

The validity of this Franck-Condon approximation to the interaction element is supported by exact numerical calculations [56,61], and by analytical arguments in §3.5 below. The use of a similar Franck-Condon approximation in the computation of the level shift by means of equation (3.8) is however open to greater risk because the significant integration range in the evaluation of $V_{nE'}$ varies as E' spans the continuum.

A second limitation on the validity of (3.36) is that the line width obtained should be small compared with the level spacing (see 3.1). A significant case not covered by (3.36) therefore arises when $H_{12}(r)$ is sufficiently large that the predissociation occurs from the upper adiabatic potential curve, $V_+(r)$, where

$$V_{\pm}(r) = \frac{1}{2}[V_1(r) + V_2(r)] \pm \frac{1}{2}\{[V_1(r) - V_2(r)]^2 + 4H_{12}^2(r)\}^{1/2} , \quad (3.37)$$

rather from the diabatic curve $V_2(r)$. The observed predissociation of ICl [85] and IBr [86, 87] are assumed to be of this type. In these circumstances equation (3.16) remains valid provided that $\chi_{2n}(r)$ and

$\chi_{1E}(r)$ in (3.32) are replaced by the bound, $\chi_{+n}(r)$, and continuum, $\chi_{-E}(r)$, wavefunctions determined by $V_+(r)$ and $V_-(r)$ respectively and the interaction term is written as [60, 88]

$$H_{+-}(r) = -H_{-+}(r) = \frac{d^2\theta}{dr} + \frac{d\theta}{dr}\frac{d}{dr}, \qquad (3.38)$$

where $\theta(r)$ is the adiabatic mixing parameter

$$\theta(r) = \arctan\left[\frac{2H_{12}(r)}{V_1(r) - V_2(r)}\right]. \qquad (3.39)$$

However the presence of a peak in $(d\theta/dr)$, and the disappearance of a crossing point precludes the use of a Franck-Condon approximation in the evaluation of $V_{nE'}$ given by (3.32).

Intermediate cases between these near diabatic and near adiabatic limits may be covered by diagonalisation of the Fano level shift matrix defined by (3.24), in order to determine the appropriate admixture (3.25) of bound states. A simpler alternative may be to seek a direct solution of the appropriate coupled differential equations, either by numerical [60] or by analytical [66] techniques. It is interesting to find that an exact model computation of this type, covering the full range of possible interaction strengths [60], shows very few resonance positions which depart significantly from these obtained by either a strict diabatic (distortion) or adiabatic approximation. This study gave however only a graphical indication of the level widths.

Finally attention may be drawn to the possibility of predissociation in the absence of a potential curve crossing (type a°, b° or c° in

Mulliken's classification [7]). Such cases may fall into either the "non-diabatic" (predissociation from $V_2(r)$) or "non-adiabatic" (predissociation from $V_+(r)$) category, and no decision can be made without examination of possible changes in the electronic state. Even in the non-diabatic case however the Franck-Condon approximation (3.36) would require careful justification in view of the absence of a crossing point.

3.4 Exact numerical results in the Franck-Condon approximation

Within the validity of the Franck-Condon approximation (3.36), a computation of the line width rests on knowledge of the exact numerical wavefunctions $\chi_{1E}(r)$ and $\chi_{2n}(r)$. Henceforth n will be taken to include a pair (v,J) of vibrational rotational quantum numbers. There is no problem such as that encountered for shape resonances (see 2.3) in locating the level position because $\chi_{2n}(r)$ may be taken as a vibrational-rotational eigenfunction of the experimental RKR bound state curve $V_2(r)$. For any given repulsive curve $V_1(r)$, the continuum state $\chi_{1E}(r)$ is also readily determined; the only problem concerns normalisation. The use of a true continuum state normalised as in (3.2) by comparison with a spherical Bessel function in the asymptotic region [89] is strictly preferable on grounds both of computional speed and flexibility, but a pseudo-continuum approximation is frequently employed [58,59], according to which

$$\chi_{1E}(r) \simeq \left(\frac{\partial N}{\partial E_N} \right)^{1/2} \chi_{1N}(r) , \qquad (3.40)$$

where $\chi_{1N}(r)$ is the N-th normalised bound wavefunction for the potential $V_1(r)$ modified by an infinite wall at some large distance. Given such wavefunctions, it is possible to vary the assumed repulsive curve until the computed line width pattern agrees with that obtained by experiment. Computations of this type have been performed for predissociations from the states of $O_2(B^3\Sigma_u^-)$ [56, 57], $N_2(b'\pi_u)$ [62], H_2 and D_2 $(D'\pi_u)$ [58], $OD(A^2\Sigma^+)$ [61] and $I_2(B^3\pi(0_u^+)$ [58, 63]. A similar calculation for the levelshift has been reported for the $B(0_u^+)$ of Se_2 [64].

The first general conclusion is that the results are indeed sensitive to the form of the repulsive curve. This is drmatically illustrated by the calculations of Reiss and Ben Aryah [57] and Murrell and Taylor [56]. Secondly the line width pattern is found, as first predicted by Rice [55], to fluctuate with v at a frequency which is high or low according to whether the intersection occurs on the attractive or repulsive branch of $V_2(r)$ (types c^+ or c^- in Mulliken's notation [7]). This behaviour may be attributed to a variation in the relative phases of the wavefunctions $\chi_{1E}(r)$ and $\chi_{2n}(r)$ at the crossing point. Hence the oscillation frequency depends on the rate of divergence of $V_1(r)$ and $V_2(r)$ above the crossing point. Typical patterns obtained by Murrell and Taylor [56) are shown in figure 3.2. The irregular nature of the fluctuations in case c^+ means that a single repulsive curve may give rise to two or more regions of strong predissociation separated by intermediate v levels for which the predissociation is weak. Theory [56, 63] suggests that the observed predissociations of $O_2(^3\Sigma_u^-)$

[90-91] and $I_2[^3\pi(0_u^+)]$ [63, 78] may be understood in this way. A second consequence is that even when the predissociation becomes so strong that all levels appear indiscernibly broad one may expect to find a few scattered sharp lines; the visible spectrum of IBr [87] is a clear example of this. The observation of such "vestigial remains" [55] would itself provide important information about the repulsive curve.

Similar fluctuations in the theoretical line width as a function of the rotational quantum number (in this case N) have been reported for the $A(^2\Sigma^+)$ of OD [61]. The variation with $N(N+1)$ is now however sufficiently slow that a more regular oscillatory pattern may be recognised (see figure 3.3). Again, within the accuracy of the measured line widths, the experimental pattern is found to be consistent with a single repulsive curve of type c^+, attributable on the evidence of the magnitude of line widths to the state $\sigma\pi\sigma^*(^4\pi)$. A similar calculations for the heterogeneous b^- predissociation from the $D('\pi_u)$ to the $B'('\Sigma_n^+)$ of H_2 [59], shows over the small J range considered $(0 < J < 10)$ no Franck-Condon contribution to the line width variation with J ; the entire variation obtained is may be attributed to the J dependence of H_{12}^o in (3.36).

The above conclusions are derived in the main for predissociation of types $c^\pm$. For an extension to cases $a^\pm$ and $b^\pm$ for which the asymptotes lie at and above the curve crossing point respectively [7], one may note that the predissociation pattern depends by the above arguments only on the local forms of the potential curves in the

crossing region. Hence one must expect an abrupt onset of the fluctuating line width pattern in place of the smooth increase shown in figure 3.2. Furthermore any consistent theory must also account for any perturbations below the predissociation limit. No calculated predissociations of types a^i, b^i and c^i, for which the crossing point coincides with the minimum in the bound state curve [7], have been reported but there appears no reason to expect a qualitatively different line width pattern. For the reasons given above, no conclusions can yet be reached for the cases designated a^o, b^o and c^o.

Turning to the level shift, Atabek and Lefebvre [64] have recently applied equation (3.8) to the interpretation of reported shifts in the $B(^3\Sigma_n^-)$ state of Se_2 [93]. The experimental results are shown to be consistent with an intersection of type c^+, but a discrepancies are found between these Fano level shifts, and the Born Oppenheimer (or adiabatic) shifts attributable to the difference between $V_2(r)$ and the lower adiabatic curve $V_-(r)$ defined by equation (3.37). The significance of these discrepancies remains to be investigated. Other features of interest are first that the calculated level shifts below the crossing point ($|F(E_v)| \simeq 8,10\ cm^{-1}$ for $v = 18,19$) exceed the corresponding widths ($\Gamma_{18} < 0.00\ cm^{-1}$, $\Gamma_{19} \simeq 0.02\ cm^{-1}$) by several orders of magnitude. Secondly a projection to levels above the crossing point indicates that the level shifts oscillate about zero as v increases. Quantitative conclusions drawn from a calculation of this type must be regarded as tentative in view of the lack of any objective criterion for the definition of an experimental level shift. Nevertheless, it is tempting to suppose that simultaneous predictions about the

behaviour of the line width and the level shift above the crossing point might lead to experimental detection of the fragmentary remains of the spectrum which could be used to refine the details of the model, even when most lines are indiscernibly diffuse.

Analytical approximations which shed some light on the above numerical conclusions are developed in the following section.

§ 3.5 Analytical approximations

Analytical approximations to the line widths and level shifts are conveniently developed in the notation indicated in figure 3.4. Here $V_i^J(r)$ denote the centrifugally corrected potential curves

$$V_i^J(r) = V_i(r) + (J + \tfrac{1}{2})^2\hbar^2/2mr^2 , \qquad (3.41)$$

in which the Langer substitution [40] of $(J + \frac{1}{2})^2$ for $J(J + 1)$, (made here for consistency with the discussion in 2.3) may be regarded as a common small semi-classical correction, $\hbar^2/8mr^2$, to the two potential curves. This substitution has no effect on the position, R, of the crossing point, with energy

$$E_{XJ} = V_1(R) + (J + \tfrac{1}{2})^2\hbar^2/2mR^2 = V_2(R) + (J + \tfrac{1}{2})^2\hbar^2/2mR^2 , \qquad (3.42)$$

or on the potential derivative difference

$$\Delta F = F_{1J} - F_{2J} , \qquad (3.43)$$

where

$$F_{iJ} = -(\partial V_i^J/dr)_{r=R} , \qquad (3.44)$$

which play an important part in the theory. ΔF is in fact independent of J, and (in the notation of figure 3.4) necessarily positive. Finally it is convenient to define two phase integral combinations

$$\phi^{+}_{vJ} = \int_{a_{1J}}^{R} k_{1J}(r)dr + \int_{R}^{b_{2J}} k_{2J}(r)dr$$

$$\phi^{-}_{vJ} = \int_{a_{2J}}^{R} k_{2J}(r)dr - \int_{a_{1J}}^{R} k_{1J}(r)dr \qquad (3.45)$$

for the interpretation of + and - predissociation respectively; here the functions $k_{1J}(r)$ and $k_{2J}(r)$ are defined by (2.2) and (2.36) with $E = E_{vJ}$ in each case. By this definition ϕ^{+}_{vJ} may be associated with the limiting form of the upper adiabatic potential defined by (3.37),

$$V^{J}_{+}(r) \simeq V^{J}_{1}(r) \qquad r < R$$

$$\simeq V^{J}_{2}(r) \qquad r > R \qquad (3.46)$$

as $H_{12}(r) \to 0$.

Franck-Condon approximations. The first analytical line width expressions are obtained in the Franck-Condon approximation, applicable for small H^{o}_{12} in (3.36). The simplest is that derived by the method of Landau and Lifshitz [84] from the semi-classical forms (2.30) and (2.32); thus

$$\chi_{2vJ}(r) = \left[\frac{2m\hbar\bar{\omega}_{vJ}}{\pi\hbar^{2}k_{2J}(r)}\right]^{1/2} \sin\left[\int_{r}^{b_{2J}} k_{2J}(r)dr + \pi/4\right]$$

$$\chi_{1EJ}(r) = \left[\frac{2m}{\pi\hbar^{2}k_{2J}(r)}\right]^{1/2} \sin\left[\int_{a_{1J}}^{r} k_{1J}(r)dr + \pi/4\right] \qquad (3.47)$$

for a predissociation of type a^+ , b^+ or c^+ . The argument involves a quadratic expansion about the crossing point for the phase of the low frequency component of the product $\chi_{2vJ}(r)\chi_{1EJ}(r)$ in (3.36), leading to the following form for the line width

$$\Gamma_{vJ} = \frac{2\hbar\bar{\omega}_{vJ}|H^o_{12}|^2}{\pi\hbar^2 v^2_{vJ}} \left| \int_{-\infty}^{\infty} \cos(\beta x^2 + \phi^+_{vJ} + \pi/2)dx \right|^2$$

$$= \Gamma^o_{vJ} \sin^2(\phi^+_{vJ} + \pi/4) , \qquad (3.48)$$

where

$$\Gamma^o_{vJ} = \frac{4\hbar\bar{\omega}_{vJ}|H^o_{12}|^2}{\hbar v_{vJ}\,\Delta F} \qquad (3.49)$$

and

$$\beta = \Delta F/2\hbar v_{vJ}$$

$$\frac{1}{2} m v^2_{vJ} = E_{vJ} - E_{xJ} . \qquad (3.50)$$

A similar expression

$$\Gamma_{vJ} = \Gamma^o_{vJ} \sin^2(\phi^-_{vJ} + \pi/4) \qquad (3.51)$$

is obtained in cases a^- , b^- or c^- .

The relation between the Fresnel integral in (3.48) and the error function [41] indicates that 95% of the integral arises from the range $|x| < 2(2/\beta)^{1/2}$. Hence equations (3.48) and (3.51) depend on the validity of the semi-classical approximations (3.47), and on the assumptions of linearity in $V^J_i(r)$ and constancy in $H_{12}(r)$ over the range

$$r = R \pm 2[\hbar v_{vJ}/\Delta F]^{1/2}$$

$$\simeq R \pm 5[(E_{vJ} - E_{xJ})/m\Delta F^2]^{1/4} , \qquad (3.52)$$

where in the second line of (3.52), the units are taken to be $r(\mathring{A})$, $E(cm^{-1})$, m(atomic mass units), $F(cm^{-1}\ \mathring{A}^{-1})$. The significance of this transition zone, the width of which increases with increasing energy, was first recognised by Bates [94]. Parameters applicable to the predissociations of $O_2(^3\Sigma_u^-)$, $I_2(B^3\pi(O_u^+))$ and $OH(A^2\Sigma^+)$ are listed in table 3.1. Note that since ΔF may become quite small for inner (a^- , b^- or c^-) curve crossings, the Franck-Condon approximation may require special justification in these cases, particularly for systems of low reduced mass.

A second analytical approximation is available to cover energies near and below the crossing point, for which overlap between the transition zone and the classical turning point regions invalidates the semi-classical approximation (3.47). One is necessarily now interested only in predissociation of types c^+ and c^- . In the latter case for example, the following Airy function [41] approximations are applicable:

$$\chi_{2vJ}(r) \simeq \left[\frac{2m\hbar\bar{\omega}_{vJ}}{\alpha_{2J}\hbar^2}\right]^{1/2} Ai[-\alpha_{2J}(r - a_{2J})]$$

$$\chi_{1EJ}(r) \simeq \left[\frac{2m}{\alpha_{1J}\hbar^2}\right]^{1/2} Ai[-\alpha_{1J}(r - a_{1J})] , \qquad (3.53)$$

where

$$\alpha_{iJ} = (2mF_{iJ}/\hbar^2)^{1/3} \qquad (3.54)$$

and the normalisations are chosen to be consistent with those in (3.47) (see Landau and Lifshitz [95]). Equations (3.53) define exact wavefunctions for the potential curves

$$V_{iJ}(r) = E_{xJ} - F_{iJ}(r - R) , \tag{3.55}$$

with $F_{iJ} > 0$. Hence the turning points at energy E_{vJ} are given by

$$a_{iJ} = (E_{vJ} - E_{xJ})/F_{iJ} . \tag{3.56}$$

With the necessary overlap integral derived in the appendix, the final line width expression may be shown to be

$$\Gamma_{vJ} = \pi\Gamma^{o}_{vJ}(v_{vJ}/v^{*}_{J})Ai^{2}[-(E_{vJ} - E_{xJ})/E^{*}_{J}] , \tag{3.57}$$

where

$$E^{*}_{J} = \frac{1}{2} mv^{*2}_{J} = (\hbar^{2}F^{2}_{1J}F^{2}_{2J}/2m\Delta F^{2})^{1/3} . \tag{3.58}$$

This formula was first given by Rice [55], and rediscovered independently by Degenkolb, Steinfeld, Wasserman and Klemperer [78] and the present author [65]. It may be shown to go over to (3.51) when $(E_{vJ} - E_{xJ}) >> E^{*}_{J}$ because [41]

$$Ai(-Z) \underset{Z \gg 1}{\sim} \pi^{-1/2}Z^{-1/4} \sin(\frac{2}{3} Z^{3/2} + \pi/4) , \tag{3.59}$$

and within the validity of (3.55)

$$\begin{aligned}\phi^{-}_{vJ} &= \frac{(2m)^{1/2}}{\hbar} \{\int_{a_{2J}}^{R} [E_{vJ} - E_{xJ} + F_{2J}(r - R)]^{1/2}dr \\ &\quad - \int_{a_{1J}}^{R} [E_{vJ} - E_{xJ} + F_{1J}(r - R)]^{1/2}dr \\ &= \frac{2}{3} [(E_{vJ} - E_{xJ})/E^{*}_{J}]^{3/2} .\end{aligned} \tag{3.60}$$

Equations (3.57), (3.58) and (3.60) (with ϕ^{+}_{vJ} in place of ϕ^{-}_{vJ}) may also be shown to be valid in case c^{+} ; the argument requires merely a reversal of sign in the argument of $\chi_{2vJ}(r)$ and the introduction of $|F_{2J}|$ in the definition of α_{2J} .

As a measure of the relative validities of (3.48) or (3.51) and (3.57) we may note that equation (3.59) reproduces the Airy function within ± 0.025 at the first maximum, Ai(-1.012) = 0.1536 , and within ± 0.005 for $Z < -3.0$. Hence as a general rule the semi-classical forms (3.48) or (3.51), which require a linear approximation to the potential only over the transition zone (see (3.52)), may be taken to be superior for $E_{vJ} - E_{xJ} > 1.5\ E^{*}_{J}$.

Before examining the physical significance of these results, we may note that an extension of the above argument to include an exponential interaction term

$$H_{12}(r) = H^{o}_{12} \exp[-\alpha(r - R)] , \tag{3.61}$$

may be shown to yield [96].

$$\Gamma_{vJ} = \pi\Gamma^{o}_{vJ}\left(\frac{v_{vJ}}{v^{*}_{vJ}}\right) \exp\left[\frac{\hbar^{2}\alpha^{3}(F_{1J} + F_{2J})}{3m\ \Delta F^{3}}\right] \mathrm{Ai}^{2}\left[-\left(\frac{E_{vJ} - E_{xJ} - E^{\ddagger}_{J}}{E^{*}_{J}}\right)\right] , \tag{3.62}$$

where

$$E^{\ddagger}_{J} = (\hbar^{2}\alpha^{2}|F_{1J}F_{2J}|2m\Delta F^{2}) . \tag{3.63}$$

The asymptotic form of (3.62),

$$\Gamma_{vJ} \simeq \Gamma^{o}_{vJ} \exp\left[\frac{\hbar^2\alpha^3(F_{1J} + F_{2J})}{3m\,\Delta F^3}\right] \cdot \sin^2\left[\frac{2}{3}\left(\frac{E_{vJ} - E_{xJ}}{E^{*}_{J}}\right)^{3/2} - \frac{\alpha^2\hbar v_J}{\Delta F} \ldots + \frac{\pi}{4}\right] , \qquad (3.64)$$

differs from that derived from (3.57) by the presence of the exponential factor and the additional phase term, $\alpha^2\hbar v_{vJ}/\Delta F$. The former is probably unimportant in most cases since $[\hbar^2\alpha^3(F_{1J} + F_{2J})/3m\Delta F^3] \simeq 10^{-3}$ for $F_{1J} = 1600$ cm^{-1}Å^{-1} , $F_{2J} = 8000$ cm^{-1}Å^{-1} , $\alpha = 1$ Å^{-1} and $m = 10$ a.m.u. for example. The form of the phase correction again underlines the significance of equation (3.52); it will be small provided the range, α^{-1} , of $H_{12}(r)$ is large compared to the width of the transition zone.

We turn now to consider the physical factors affecting the line width variation with v at given J . Figure 3.5 gives a comparison between the predictions of equations (3.48) and (3.57) and the computed values of Murrell and Taylor [56]. The properties of the Airy function [41] indicate that the line width envelope should reach a maximum at $E_{xJ} + 1.019\ E^{*}_{J}$, with a point of inflexion at the crossing point and an exponential decrease

$$\Gamma_J \simeq \frac{1}{4}\left|\Gamma^{o}_{vJ}\right| \exp\left[-\frac{4}{3}\left(\frac{E_{xJ} - E_{vJ}}{E^{*}_{J}}\right)^{3/2}\right] , \qquad (3.65)$$

for $E - E_{vJ} < -E^{*}_{J}$. The much slower decline at higher energies is governed according to equation (3.49) by the ratio $(\bar{\omega}_{vJ}/v_{vJ})$; note

that since the local energy spacing, $\hbar\bar{\omega}_{vJ}$, must vanish at the dissociation limit, even when the predissociation appears very strong, a discrete spectrum must be regained as the energy increases.

The frequency of oscillations within this envelope depends on the energy variation of the appropriate phase integral ϕ^{+}_{vJ} or ϕ^{-}_{vJ} . Seen in this light the oscillations may be attributed to semi-classical interference [97] between the two possible escape trajectories associated with transitions at the crossing point during outward or inward motion respectively, the latter being followed by reflection at the classical turning point on the repulsive curve. Hence the line width pattern is in effect an interferogram for the nett path difference $b_{2J} - a_{1J}$ or $a_{1J} - a_{2J}$ in cases + or - respectively. This idea is fully exploited in§3.6.

Seen in more concrete terms, it is clear from figure 3.4 and from the definitions (3.45) that the energy dependence of $\phi^{\pm}_{vJ}$ must depend on the rate of divergence of the potential curves. In case c^{+} the necessary derivative may in fact be associated by the usual semi-classical arguments (see (2.36)) with a hypothetical energy spacing $h\bar{\omega}^{(+)}$ in the potential curve $V^{J}_{+}(r)$ defined by (3.46);

$$\left(\frac{\partial\phi^{+}_{vJ}}{\partial v}\right) = \left(\frac{\partial E_{vJ}}{\partial v}\right)\left(\frac{\partial\phi^{+}_{vJ}}{\partial E_{vJ}}\right) = \pi\left(\frac{\hbar\bar{\omega}_{vJ}}{\hbar\bar{\omega}^{(+)}}\right) . \qquad (3.66)$$

This means that close to the dissociation limit, where both $h\bar{\omega}_{vJ}$ and $h\bar{\omega}^{(+)}$ must depend only on the long range form of $V^{J}_{2}(r)$ [98],

$$\frac{\partial\phi^{+}_{vJ}}{\partial v} = \pi . \qquad (3.67)$$

The factors affecting the line width variation with J may also be understood in the light of equations (3.48), (3.51) and (3.57). The overriding consideration is that the energy difference in (3.57) varies as

$$E_{vJ} - E_{xJ} = E_v - E_{xo} + [hcB_v - \hbar^2/2mR^2]J(J + 1) . \quad (3.68)$$

Hence for vibrational levels near the crossing point the line width must increase or decrease with increasing J in cases c^+ or c^- respectively. Similarly the phase terms ϕ^+_{vJ} and ϕ^-_{vJ} may be seen to be increasing and decreasing functions respectively, with $(\partial\phi^+_{vJ}/\partial J)$ approximately given by [67]

$$\left(\frac{\partial\phi^+_{vJ}}{\partial J}\right) = (2J + 1)\pi\left(\frac{B_v - B^{(+)}(E_v)}{\hbar\bar{\omega}^{(+)}}\right) , \quad (3.69)$$

where $h\bar{\omega}^{(+)}$ and $B^+(E_v)$ are respectively the hypothetical vibrational spacing and rotational constant at the measured energy E_v for the potential curve $V_+(r)$.

Finally the effects of isotopic substitution may be considered. It is convenient to make comparisons at a common absolute energy and at equivalent mass reduced J values (having a common value of $J(J + 1)/m$) . With these provisos, the envelope function Γ^o_{vJ} in (3.48) and (3.51) carry however a factor $m^{1/2}$. Hence when regarded as a function of energy the onset of strong predissociation will appear sharper and the subsequent oscillation frequency will be increased at higher mass values.

General approximations. A quite different type of semi-classical theory, analogous to that described in 2.2 has also been developed [66]. This relies on the use of semi-classical connection formulae (equation (18) of reference [66]) for the Stuckelberg-Landau-Zener [99-101] curve crossing model. The results are therefore again limited by the approximations of constant velocity, constant interaction and linear potential curve expansions over the transition zone defined by (3.52). Being non-perturbative, however, the method carries no restriction on the magnitude of H_{12}^{o} . Furthermore it yields analytical expressions both for the line width and for the level shift.

The results may be expressed in terms of one or other of the Landau-Zener transition probabilities [99-101]

$$P_{vJ} = 1 - \exp[-2\pi H_{12}^{o\,2}/\hbar v_{vJ}\Delta F]$$

$$\tilde{P}_{vJ} = 1 - P_{vJ} = \exp[-2\pi H_{12}^{o\,2}/\hbar v_{vJ}\Delta F] \; ; \qquad (3.70)$$

P_{vJ} gives the probability of a transition from $V_2^J(r)$ to $V_1^J(r)$ on a single passage through the crossing zone, while P_{vJ} refers to a transition from one adiabatic curve $V_+^J(r)$ or $V_-^J(r)$ to the other. Predissociations of measurable line width are predicted when either

$$P_{vJ} \ll 1 \qquad \text{or} \qquad \tilde{P}_{vJ} \ll 1 \; . \qquad (3.71)$$

The former correspond to what we have termed the non-adiabatic predissociations discussed in the first part of this section, and formulae for the line widths are identical with those given by (3.48) and (3.51). The associated level shifts may be written

$$\Delta E_{vJ} = \frac{1}{2}\Gamma^{o}_{vJ}\sin(\phi^{+}_{vJ}+\frac{\pi}{4})\cos(\phi^{+}_{vJ}+\frac{\pi}{4}) \qquad (3.72)$$

in cases a^{+}, b^{+} or c^{+}, and

$$\Delta E_{vJ} = -\frac{1}{2}\Gamma^{o}_{vJ}\sin(\phi^{-}_{vJ}+\frac{\pi}{4})\cos(\phi^{-}_{vJ}+\frac{\pi}{4}) \qquad (3.73)$$

in cases a^{-}, b^{-} or c^{-}.

The second inequality in (3.71) refers to predissociation from the upper adiabatic potential curve $V^{J}_{+}(r)$ defined by (3.37), such as that observed in the visible spectra of ICl [85] and IBr [86-87]. It is convenient to coin the notations $\tilde{a}^{\pm}$, $\tilde{b}^{\pm}$ or $\tilde{c}^{\pm}$ to distinguish predissociations of this type from the more common non-adiabatic phenomena. The expressions for the line width and leve now become

$$\Gamma_{vJ} = \tilde{\Gamma}^{o}_{vJ}\cos^{2}\phi^{(2)}_{vJ} \qquad (3.74)$$

$$\Delta E_{vJ} = \frac{1}{2}\tilde{\Gamma}^{o}_{vJ}\sin\phi^{(2)}_{vJ}\cos\phi^{(2)}_{vJ}\ , \qquad (3.75)$$

where

$$\Gamma^{o}_{vJ} = 2\left(\frac{\hbar\bar{\omega}_{vJ}}{\pi}\right)\exp[-2\pi H^{o}_{12}{}^{2}/\hbar v_{vJ}\Delta F]\ , \qquad (3.76)$$

and

$$\phi^{(2)}_{vJ} = \int_{a_{2J}}^{b_{2J}} k_{2J}(r)dr = \frac{(2m)^{1/2}}{\hbar}\int_{a_{2J}}^{b_{2J}}[E_{vJ}-V^{J}_{2}(r)]^{1/2}dr\ . \qquad (3.77)$$

Note that $\hbar\bar{\omega}_{vJ}$ now refers to the level spacing in $V^{J}_{+}(r)$. The ratio of the line width to the local energy spacing, $\Gamma^{o}_{vJ}/\hbar\bar{\omega}_{vJ}$, is therefore predicted to oscillate within an increasing envelope as indicated schematically in figure 3.6. The disappearance of $\hbar\bar{\omega}_{vJ}$ at the

dissociation limit however again implies that the lines must eventually become sharp.

These equations raise several points of interest. First the inequalities (3.68) give quantitative tests for the validity of a non-diabatic or a non-adiabatic description. Secondly equations (3.74) and (3.77) predict a sharp line in the spectrum whenever a bound level of $V_+^J(r)$ coincides with a bound level of $V_2^J(r)$ because, by the Bohr quantisation condition (2.34), $\phi_{vJ}^{(2)} = (n + \frac{1}{2})\pi$ under these conditions. This behaviour is strikingly demonstrated by the visible spectrum of IBr [86, 87]. Finally the intimate connection between the line width and the level shift which implies zero level shift for the sharp resonances under all conditions may have some general significance. Although this behaviour is not confirmed by the numerical results of Atabek and Lefebore [64] possibly due to strong curvature in the repulsive curve $V_1(r)$, it means within the validity of the present model that the measured energy variation with J contains a systematic error in the rotational constant. Thus at the sharp resonance points

$$\left[\frac{\partial E_{vJ}}{\partial J(J+1)}\right] = hcB_v \pm \frac{1}{2}\Gamma^o_{vJ}\left(\frac{\partial \phi^{\pm}_{vJ}}{\partial J(J+1)}\right) \qquad (3.78)$$

for non-diabatic predissociations, while

$$\left[\frac{\partial E_{vJ}}{\partial J(J+1)}\right] = hcB_v - \frac{1}{2}\tilde{\Gamma}^o_{vJ}\left(\frac{\partial \phi^{(2)}_{vJ}}{\partial J(J+1)}\right) \qquad (3.79)$$

in the non-adiabatic case. The behaviour of $[\partial\phi^{\pm}_{vJ}/\partial J(J+1)]$ has been discussed above (see 3.69)); the application of similar arguments shows that

E

$$\frac{\partial \phi_{vJ}^{(2)}}{\partial J(J+1)} = \pi \left[\frac{B_v - B^{(2)}(E_v)}{\hbar \bar{\omega}^{(2)}} \right] . \qquad (3.80)$$

This term will be negligible in cases $\bar{a}$, $\bar{b}$, and $\bar{c}$ because the minima in $V_+^J(r)$ and $V_2^J(r)$ must coincide, while $[\partial \phi^{(2)}/\partial J(J+1)]$ will clearly be negative in cases $\tilde{\bar{a}}^+$, $\tilde{\bar{b}}^+$, and $\tilde{\bar{c}}^+$. Hence equations (3.69) and (3.78)-(3.80) carry a general prediction that anomalies of this type must lead to an increase in the apparent B value. The magnitude of this increase clearly depends on Γ_{vJ}^o or $\tilde{\Gamma}_{vJ}^o$. It must be negligible for predissociations which are weak to the extent that all rotational lines are observed, but it may become significant in the interpretation of fragmentary systems, such as that shown by IBr [86, 87], which contains only a few measurably sharp lines.

§ 3.6 Direct inversion of the line width pattern

A direct method for determination of the repulsive curve $V_1(r)$ and the interaction strength H_{12}^o has been developed [65, 67, 68] from the analytical theory of the previous section. Closely akin to the RKR method [102, 103] of bound state spectroscopy, it is based on recognition that the phase integrals $\phi_{vJ}^{\pm}$ in equations (3.45), (3.48) and (3.51) contain the same information about the upper branches of $V_1(r)$ and $V_2(r)$ in figure (3.4), as that supplied by the Bohr quantisation condition $(\phi = (n + \frac{1}{2})\pi)$ for a normal bound state curve. The only difference is that the energy dependence of $\phi_{vJ}^{\pm}$ must be extracted from the line width pattern. Once this function is known however the separation between the turning on $V_1(r)$ and $V_2(r)$ at energy U is given by [65, 68]

$$b_2(U) - a_1(U) = \frac{\hbar}{\pi}\left(\frac{2}{m}\right)^{1/2}\int_{E_{xo}}^{U}\left(\frac{\partial\phi_{vo}^{+}}{\partial E}\right)\frac{dE}{(U-E)^{1/2}} \qquad (3.81)$$

in case c^+ or [68]

$$a_1(U) - a_2(U) = \frac{\hbar}{\pi}\left(\frac{2}{m}\right)^{1/2}\int_{E_{xo}}^{U}\left(\frac{\partial\phi_{vo}^{-}}{\partial E}\right)\frac{dE}{(U-E)^{1/2}} \qquad (3.82)$$

in case c^- . Since the turning point $a_2(U)$ or $b_2(U)$ is normally known from an experimental RKR curve $V_2(r)$, equations (3.81) or (3.82) are sufficient to determine $V_1(r)$. Similarly the J dependence of $\phi_{vJ}^{\pm}$ may be used [67] to obtain an analogue of the second RKR equation, but this is unlikely to be of practical value except for confirmatory purposes.

The determination of $\phi_{vo}^{\pm}$ rests primarily on location of the crossing point E_{xo} . As a first step it is convenient to rewrite equations (3.48), (3.51) and (3.57) in the form

$$\gamma_{vo} = (\Gamma_{vo}/h\bar{\omega}_{vo})^{1/2} = \pi^{1/2}\,KE_o^{*-1/4}\,Ai\left[-\left(\frac{E_{vo}-E_{xo}}{E_o^*}\right)\right]$$

$$\text{for } E_{vo} \simeq E_{xo} \qquad (3.83)$$

$$= K(E_{vo}-E_{xo})^{-1/4}\sin(\phi_{vo}+\frac{\pi}{4}+n_v\pi)$$

$$\text{for } E_{vo} >> E_{xo}\,, \qquad (3.84)$$

where

$$\bar{\omega}_{vo} = \frac{\partial G_v}{\partial v} . \qquad (3.85)$$

γ_{vo} and E_{vo} are therefore experimental quantities; the unknowns are K, E_o^*, E_{xo}, $\phi_{vo}^{\pm}$ and the integers n_v. Two equations for K, E_o^* and E_{xo} may be taken from the position and magnitude of the first Airy function maximum estimated from three neighbouring line widths (or from the greatest measured with in the absence of adequate data [68]); the equations are

$$\gamma^{max} = \pi^{1/2} Ai(-1.01879) K E_o^{*-1/4} = 0.94943 K E_o^{*-1/4} \qquad (3.86)$$

$$E^{max} - E_{xo} = 1.01879 E_o^* . \qquad (3.87)$$

For a third equation it may be assumed that the maximum product $\gamma_{vo}(E_{vo} - R_{xo})^{1/4}$ in the higher energy region corresponds with a sinusoidal maximum (a crude estimate of E_{xo} will suffice for this purpose). Hence

$$K = [(E_{vo} - E_{xo})^{1/4} \gamma_{vo}]_{max} . \qquad (3.88)$$

As an alternative, depending on the quality of the data one might employ four measured line widths in the Airy function region to determine the first maximum and a point of inflexion in the line width envelope, the latter being taken to determine the crossing point. Preliminary estimates of K, E_{xJ} and E_J^* obtained in this way may be improved by comparison between computed and measured line width patterns in the Airy region. The phases in this region are now given by equation (3.60);

$$\phi_{vo}^{\pm} = \frac{2}{3}\left[(E_{vo} - E_{xo})/E_o^*\right]^{3/2} . \qquad (3.89)$$

It remains to eliminate ambiguities of $n_v\pi$ in the phases obtained by inversion of (3.84). A plot of

$$\Delta\phi_{vo} = \phi_{vo}^{+} - \int_R^{b_2} k_2(r)dr \qquad \text{in case } c^+$$

$$= \int_{a_2}^{R} k_2(r)dr - \phi_{vo}^{-} \qquad \text{in case } c^- \qquad (3.90$$

against $(E_{vo} - E_{xo})^{3/2}$ is recommended for this purpose. Here $k_2(r)$ is derived from the known RKR curve $V_2(r)$ by means of equations (2.2) and (2.6). This graph is suggested by a linear expansion for the potential $V_1(r)$ (see equation (3.60)); the present model requires that it should pass through and behave linearly at the origin. Not only will this graph remove the necessary ambiguities of $n_v\pi$, it may also be used to smooth out experimental uncertainties in the line width, to refine the location of the crossing point in cases offering insufficient data in the Airy region, and to combine data for different isotopic substituents because the phases in (3.90) all vary at a given energy as $m^{1/2}$.

Finally one may note an internal check on the consistency of the method, because the value of E_o^* used to fit the data in the Airy function region, may be compared with that deduced from (3.58) in terms of the slopes F_{1o} and F_{2o} derived from the calculated curves. A valuable general property of the method is its stability. Refinement of a preliminary analysis of the magnetic flourescence quenching data for $I_2[B^3\pi(0_u^+)]$ [63, 78], by means of the $\Delta\phi$ plot (figure 3.7) is found to change the crossing region parameters (E_{xo}, E_o^* and K) from (306 cm^{-1},

468 cm^{-1} and 3.217) to (475 cm^{-1}, 340 cm^{-1} and 3.162) , but to alter the turning points on $V_1(r)$ by -.002 Å for v = 6,11 , ±.001 Å fo v = 14,16,18,21,24,28 and 32 and -.004 Å for v = 38 . There is insufficient experimental data near the predicted crossing point for a meaningful consistency check on the value of E_o^* . A comparison between the refined potential curve $V_1(r)$ and the form deduced by Chapman and Bunker [63] from a numerical Franck-Condon calculation is given in figure 3.8.

This direct inversion procedure has been successfully applied to the computed predissociation data for $O_2(^3\Sigma_u^-)$ [65] and to experimental data for $OD(A^2\Sigma^+)$ [67] and $I_2(B^3\pi(O_u^+))$ [68]. The resulting repulsive potential curves are closely comparable to those deduced by numerical Franck-Condon calculations (see figure 3.8). The advantagesof the direct approach are speed and flexibility, since the only prior assumption is of linearity in the potential curves over the transition zone. This suggests its general future use as a preliminary to the potentially more exact numerical Franck-Condon procedure.

§3.7 Summary and conclusions

It has been amply confirmed by practical tests that a pattern of measured predissociation line widths (or lifetimes) contains sufficient information to determine the repulsive curve $V_1(r)$, over the predissociation region, and also the interaction potential H_{12}^o . The lineshape envelope as illustrated in figures 3.2, 3.5 and 3.6 suffices to determine the predissociation type. The frequency of oscillations within this envelope depends, in the normal non-diabatic case, on the

rate of divergence of the two potential curves above the crossing point. Similar fluctuations in the case of predissociation from the upper adiabatic curve $V_+(r)$ depend on the shape of $V_2(r)$. Subsidiary fluctuations with J are also predicted, at a frequency roughly governed according to equations (3.69) and (3.80) by the displacement between the crossing point and the bound state potential minimum. An analytical characterisation of these fluctuations has led to development of the direct inversion procedure described in 3.6. The interpretation of a well developed predissociation pattern in cases $c^{\pm}$ is therefore now a routine matter.

Preliminary attention has also been directed towards the concurrent levelshift. Specifically, at energies below the crossing point one may expect to observe shifts which are several magnitudes larger than the line width. However it is not yet clear whether these should be interpreted as Fano shifts in the sense of equation (3.8), or simply as adiabatic shifts due to an avoided curve crossing. The sign of such shifts is negative for crossings of the $+$ type, and may be expected by the adiabatic interpretation to be positive in the opposite case. At energies above the crossing point the levelshift is predicted to oscillate about a mean value zero in such a way that within the validity of a Landau-Zener model a small positive additional term is predicted in the rotation constant.

Turning to the future one may expect to see the direct connection between perturbations and predissociations of types a and b more fully exploited, particularly when the whole spectrum is substantially discrete. A more challenging situation for the theoretician arises when the predissociation is strong in the spectroscopic sense that

all discrete structure appears lost, but weak to the extent that the line width is small compared with the vibrational spacing. Here one might hope that analysis of low-energy level-shifts or possible perturbations might lead, via the appropriate repulsive curve, to the prediction and detection of fragmentary remains of the spectrum at the oscillation minima in figures 3.5 and 3.6.

Another possibility is that spectroscopic predictions of strong predissociation into states which correlate with ground state atoms might stimulate the observation of such resonances by scattering techniques, as a complement to the achievements of Bernstein [1966], Stwalley et al. [3], and Schulte et al [4] in the somewhat simpler shape resonance field. A possible example might be the IBr system [86, 87], but there may be others which are preferable on experimental grounds.

ACKNOWLEDGEMENT

The author is grateful for the hospitality of The Theoretical Chemistry Institute, University of Wisconsin during the preparation of this report. He wishes particularly to acknowledge the interest and advice of Professor R. B. Bernstein.

REFERENCES

1. See in particular references [63, 78] below.

2. Bernstein, R. B., 1966, Phys. Rev. Lett. 16, 385.

3. Stwalley, W. C., Niehaus, A., and Herschbach, D. R., in Fifth International Conference on the Physics of Electronic and Atomic Collisions, Leningrad, 1967, Abstracts of Papers, edited by Flaks, I. P., and Solovoyov (Nauka, Leningrad, 1967) p. 639.

4. Schutte, A., Bassi, D., Tommasini, F., and Scoles, G., 1972, Phys. Rev. Lett., 29, 979.

5. Peek, R. A., 1973, Physica 64, 93.

6. Herzberg, G., 1950, Spectra of Diatomic Molecules (Van Nostrand).

7. Mulliken, R. S., 1960, J. Chem. Phys. 33, 247.

8. Kronig, R. deL., 1932, Z. Phys. 75, 468.

9. Van Vleck, J. H., 1932, Phys. Rev., 40, 544.

10. Gaydon, A. G., 1968, Dissociation Energies and Spectra of Diatomic Molecules, 3rd Edition (Chapman and Hall).

11. See also Gersch, M. E., and Bernstein, R. B., 1969, Chem. Phys. Lett., 4, 221 for a computed total cross-section for the scattering of two H(1S) atoms.

12. See Alfaro, V. de., and Regge, T., 1965, Potential Scattering (North-Holland).

13. Ford, K. W., Hill, D. L., Wakano, M., and Wheeler, J. A., 1959, Ann. Phys. 7, 239.

14. Buckingham, R. A., and Fox, J. W., 1962, Proc. Roy Soc. A267, 102.

15. Buckingham, R. A., Fox, J. W., and Gal, E., 1965, Proc. Roy. Soc. A284, 237.

16. Bernstein, R. B., Curtiss, C. F., Imam Rahajoe, S., and Wood, W. T., 1966, J. Chem. Phys. 44, 4072.

17. Waech, T. G., and Bernstein, R. B., 1967, J. Chem. Phys. 46, 4905.

18. Allison, A. C., 1969, Chem. Phys. Lett. 3, 371.

19. Jackson, J. L., and Wyatt, R. E., 1970, Chem. Phys. Lett. 4, 643.

20. LeRoy, R. J., and Bernstein, R. B., 1971, J. Chem. Phys. 54, 5114.

21. Bain, R. A., and Bardsley, J. N., 1971, J. Chem. Phys. 55, 4535.

22. Buckingham, R. A., and Dalgarno, A., 1952, Proc. Roy. Soc. A213, 506.

23. Berry, M. V., 1966, Proc. Phys. Soc. 88, 285.

24. Dubrovskii, G. V., 1964, Optika Specktrosk. 17, 771 (English translation: 1964, Optics Spectrosc. 17, 416).

25. Livingston, P. M., 1966, J. Chem. Phys. 45, 601.

26. Herm, R. R., 1967, J. Chem. Phys. 47, 4290.

27. Miller, W. H., 1968, J. Chem. Phys. 48, 1651.

28. Connor, J. N. L., 1968, Mol. Phys. 15, 621; 1969, ibid 16, 525.

29. Dickinson, A. S., 1970, Mol. Phys. 18, 441.

30. Fröman, N., and Fröman, P. O., 1970, Nucl. Phys. A147, 606.

31. Bayliss, W. E., 1970, Phys. Rev. 1, 990.

32. Connor, J. N. L., 1972, Mol. Phys. 23, 717.

33. Eisbud, L., 1948, dissertation Princeton University.

34. Wigner, E. P., 1955, Phys. Rev. 98, 145.

35. Smith, F. T., 1960, Phys. Rev. 118, 349; Erratum, 1960, 119, 2098.

36. Dirac, P. A. M., 1958, The Principles of Quantum Mechanics, 4th Edition (Oxford).

37. See Messiah, A., 1962, Quantum Mechanics (N. Holland, Amsterdam).

38. Siegert, A. F. J., 1939, Phys. Rev. 56, 750.

39. See Jeffreys, B. S., 1961, in Quantum Theory, 10-1, Elements: edited by D. R. Bates (Academic Press).

40. Here we employ the standard Langer correction of molecular scattering theory in replacing $J(J+1)$ by $(J+\frac{1}{2})^2$; see Langer, R. E., 1937, Phys. Rev. 51, 669.

41. Abramowitz, M., and Stegun, I. A., 1965, Handbook of Mathematical Functions (Dover).

42. Landau, L. D., and Lifshitz, E. M., 1958, Quantum Mechanics (Adison-Wesley).

43. Allison, A. C., and Dalgarno, A., 1971, J. Chem. Phys. 55, 4342.

44. Smith, A. L., 1971, J. Chem. Phys. 55, 4344.

45. Connor, J. N. L., 1968, Mol. Phys. 15, 37.

46. Miller, S. C., and Good, R. H., 1953, Phys. Rev. 91, 174; see also Hecht, C. E., and Mayer, J. E., 1957, Phys. Rev. 106, 1156, and Dingle, R. B., 1956, Appl. Sci. Res. B5, 345.

47. Soop, M., 1965, Ark. Fys., 30, 217.

48. Johnson, B. R., Balint-Kurti, G. G., and Levine, R. D., 1970, Chem. Phys. Lett. 1, 268.

49. Mahan, G. D., and Lapp, M., 1969, Phys. Rev. 179, 19.

50. LeRoy, R. J., 1971, University of Wisconsin Theoretical Chemistry Institute Report WIS-TCI-387.

51. See for example Farkas, L., and Levy, S., 1933, Z. Phys. 84, 195, on AlH , and Porter, T. L., 1962, J. Opt. Soc. Am. 52, 1201 on HgH.

52. Bernstein, R. B., 1966, Phys. Rev. Lett. 16, 385.

53. Byrne, M. A., Richards, W. G., and Horsley, J. A., 1967, Mol. Phys. 12, 273.

54. Horsley, J. A., and Richards, W. G., 1969, J. Chem. Phys. 66, 41.

55. Rice, O. K., 1933, J. Chem. Phys. 1, 375.

56. Murrell, J. N., and Taylor, J. M., 1969, Mol. Phys. 16, 609.

57. Riess, I. M., and Ben Aryeh, Y., 1969, J. Quant. Spect. Radiat. Transfer 9, 1463.

58. Chutjian, A., 1969, J. Chem. Phys. 51, 5414.

59. Fiquet-Fayard, F., and Gallais, O., 1970, Mol. Phys. 20, 527.

60. Levine, R. D., Johnson, B. R., and Bernstein, R. B., 1969, J. Chem. Phys. 50, 1694.

61. Czarny, J., Felenbok, P., Lefebvre-Brion, H., 1971, J. Phys. B. 4, 124.

62. Leoni, M., and Dressler, K., 1971, J. Appl. Math. and Phys. 22, 794.

63. Chapman, G. D., and Bunker, P. R., 1972, J. Chem. Phys. 57, 2951.

64. Atabek, O., and Lefebvre, R., 1972, Chem. Phys. Lett. 17, 167.

65. Child, M. S., 1970, J. Mol. Spect. 33, 487.

66. Bandrauk, A. D., and Child, M. S., 1970, Mol. Phys. 19, 95.

67. Ramsay, D. S., and Child, M. S., 1971, Mol. Phys. 22, 263.

68. Child, M. S., 1973, J. Mol. Spect. (in press).

69. Fano, U., 1961, Phys. Rev. 124, 1866.

70. Feshbach, H., 1958, Ann. Phys. 5, 357.

71. Van Santen, R. A., 1971, Physica 62, 51.

72. See Phillips, E. G., 1957, Functions of a Complex Variable (Oliver and Boyd).

73. Herzberg, G., and Jungen, Ch., 1972, J. Mol. Spect. 41, 425.

74. Beulter, H., 1935, Z. Phys. 93, 177.

75. See Caplan, C. E., and Child, M. S., 1972, Mol. Phys. 23, 249.

76. Mulliken, R. S., 1937, J. Phys. Chem. 41, 5.

77. Turner, L. A., 1930, Z. Phys. 65, 464.

78. Degenkolb, E. O., Steinfeld, J. I., Wassermann, E., and Klemperer, W., 1969, J. Chem. Phys. 51, 615.

79. Turner, L. A., 1931, Phys. Rev. 38, 574.

80. Turner, L. A., 1933, Phys. Rev. 41, 627.

81. Steinfeld, J. I., and Klemperer, W., 1965, J. Chem. Phys. 42, 3475.

82. Steinfeld, J. I., 1966, J. Chem. Phys. 44, 2740.

83. Zener, C., 1933, Proc. Roy. Soc. A140, 660.

84. See Landau, L. D., and Lifshitz, E. M., [42] §8.7.

85. Brown, W. G., and Gibson, G. E., 1932, Phys. Rev. 40, 529.

86. Brown, W. G., 1932, Phys. Rev. 42, 355.

87. Selin, L. E., 1962, Arkiv för Fys. 21, 529.

88. Berry, R. S., 1957, J. Chem. Phys. 27, 1288.

89. Comparisons of possible computational methods have been given by Allison, A. C., 1970, J. Computing Phys. 6, 378, and Gordon, R. G., 1971, in Methods in Computing Physics 10, edited by Alder, B., Fernbach, S., and Rotenberg, M. (Academic Press) p. 81.

90. Wilkinson, P. G., and Mulliken, R. S., 1957, Astrophys. J., 125, 594.

91. Carroll, P. K., 1959, Astrophys. J. 129, 794.

92. Ackerman, M., and Biaume, F., 1970, J. Mol. Spect. 35, 73.

93. Barrow, R. F., Chandler, G. G., and Meyer, C. B., 1960, Phil. Trans. Roy. Soc. 260, 395.

94. Bates, D. R., 1960, Proc. Roy. Soc. A257, 22.

95. See Landau and Lifshitz [42] §47.

96. Child, M. S., 1972, Mol. Phys. 23, 269.

97. Miller, W. H., 1970, J. Chem. Phys. 53, 1949.

98. LeRoy, R. J., and Bernstein, R. B., 1970, J. Chem. Phys. 52, 3869.

99. Stuckelberg, E. C. G., 1932, Helv. Phys. Acta. 5, 369.

100. Landau, L. D., 1932, Phys. Z. Sow 1, 46.

101. Zener, C., 1932, Proc. Roy. Soc. A137, 696.

102. Rydberg, J. R., 1931, Z. Phys. 73, 376.

103. Klein, O., 1932, Z. Phys. 76, 226.

APPENDIX: THE AIRY FUNCTION OVERLAP INTEGRAL

The integral

$$I = \int_{-\infty}^{\infty} \mathrm{Ai}[\gamma(r - c)]\, \mathrm{Ai}[\gamma'(r - c')]dr \,, \tag{A.1}$$

with $\gamma > \gamma'$ may be evaluated by use of the integral representation [41]

$$\mathrm{Ai}(z) = \frac{1}{\pi}\int_0^{\infty} \cos\left(\frac{1}{3}u^3 + uz\right)du = \frac{1}{2\pi}\int_{-\infty}^{\infty} \exp\left[\frac{iu^3}{3} + iuz\right]du \,. \tag{A.2}$$

Thus

$$\begin{aligned} I &= \frac{1}{(2\pi)^2}\int_{-\infty}^{\infty}\int_{-\infty}^{\infty}\int_{-\infty}^{\infty} \exp\left\{\frac{i}{3}(u^3 + v^3) + i(\gamma u + \gamma' v)r \right. \\ &\qquad \left. - i(u\gamma c + v\gamma' c')\right\}drdudv \\ &= \frac{1}{2\pi}\int_{-\infty}^{\infty}\int_{-\infty}^{\infty} \exp\left\{\frac{i}{3}(u^3 + v^3) - i(u\gamma c + v\gamma' c')\right\}\delta(\gamma u + \gamma' v)dudv \\ &= \frac{1}{2\pi\gamma}\int_{-\infty}^{\infty} \exp\left\{\frac{i}{3}[1 - (\gamma'/\gamma)^3]v^3 - i(c' - c)\gamma' v\right\}dv \\ &= (\gamma^3 - \gamma'^3)^{-1/3}\, \mathrm{Ai}\left[\frac{\gamma\gamma'(c - c')}{(\gamma^3 - \gamma'^3)^{1/3}}\right] \,. \end{aligned} \tag{A.3}$$

Here the identity [36]

$$\int_{-\infty}^{\infty} \exp ikr\, dr = 2\pi\, \delta(k) \tag{A.4}$$

has been used to obtain the second line of (A.3).

CAPTIONS FOR TABLES

2.1 Values of the level shift function $\phi(\varepsilon)$ in the associated quadratic approximation (equation (2.63)).

$$\phi(-\varepsilon) = -\phi(\varepsilon) .$$

$$\phi(\varepsilon) \simeq \varepsilon^{-1}/24 + 7\varepsilon^{-3}/2880 \qquad \text{for } \varepsilon > 1 .$$

2.2 Comparative resonance positions and widths for the Lennard-Jones model, with the potential parameters employed by Bernstein et al. [6]. ε_o denotes the well depth. Energies and widths are expressed as a fraction of the well depth.

2.3 Comparative resonance positions and widths for the H_2 ground state [10]. Values under BC(Airy) refer to the Airy function boundary condition at the outermost turning point.

2.4 Simple, $\Gamma^{(o)}$, and improved, $\Gamma^{(1)}$, semi-classical level widths for the H_2 ground state. q and t in the final columns are the parameters for the associated Morse approximation; note that $\pi qt >> 1$.

3.1 Parameters for some observed predissociations.

CAPTIONS FOR FIGURES

2.1 The condition for possible predissociation by rotation.

2.2 Notation for the semi-classical theory. a, b and c denote the classical turning points. Capital letters denote the amplitudes of travelling waves, with primes and double primes used to indicate outgoing and incoming motion respectively.

3.1 The Beutler-Fano line-shape for $q = 3$ (see equation (3.23)). The corresponding form for $q = -3$ is obtained by reflection in the origin.

3.2 Computed linewidth variations with v [57] for cases c^+ (upper diagram) and c^- (lower diagram). Note the contrast between the irregular fluctuations in case c^+, with the smooth variation in case c^-. Compare also figure 3.4.

3.3 Computed linewidth variations with v and J [61] for homogeneous predissociation from the $A(^2\Sigma^+)$ of OH.

3.4 Notation for the semi-classical theory (a) in case c^+, and (b) in case c^-.

3.5 A comparison between the computed linewidth pattern [57] for predissociation of $O_2(^3\Sigma_u^-)$ and the analytical expressions (3.48) (dashed line) and (3.57) (solid line). Note that a satisfactory Airy function representation (solid line) as far as the third minimum should be regarded as atypical. Curvature in the potential

energy functions may normally be expected to cause deviations between the semi-classical (dashed line) and the Airy function behaviour at a point between the first maximum and the first minimum (see text).

3.6 Schematic line width variation with v for a $\tilde{c}^{+}$ case of non-adiabatic predissociation from the potential curve $V_{+}(r)$. Vertical lines indicate the line widths.

3.7 Refinement of the magnetic flourescence quenching data for the $B[^{3}\pi(0_{u}^{+})]$ state of I_2 . The point $v = 6$ is derived <u>a postiori</u> from equation (3.60) with E_{o}^{*} given in terms of the slope of the inverted curve by equation (3.58).

3.8 Comparison between the repulsive curve $V_1(r)$ deduced for the $B^{3}\pi(0_{u}^{+})$ state of I_2 by a numerical Franck-Condon calculation [63] and the points obtained by the direct inversion method.

TABLE 2.1

ε	$\phi(\varepsilon)$	ε	$\phi(\varepsilon)$
0	0	0.6	0.080
0.1	0.137	0.7	0.068
0.2	0.150	0.8	0.058
0.3	0.135	0.9	0.051
0.4	0.115	1.0	0.045
0.5	0.096		

TABLE 2.2

ℓ	E_{nJ}			Γ_{nJ}		
	Phase Shift[a]	BB[b]	JWKB[c]	Phase Shift[a]	BB[b]	JWKB[c]
118	.31005	.31004	.31003		1.2×10^{-17}	1.0×10^{-17}
197	.31005	.31008	.31007		9.6×10^{-28}	9.0×10^{-28}
25	.34855	.34862	.34846	6.2×10^{-4}	6.0×10^{-4}	6.7×10^{-4}
77	.34935	.34935	.34938		6.9×10^{-8}	8.0×10^{-8}
128	.35005	.35007	.35007		2.0×10^{-11}	2.0×10^{-11}
123	.38967	.38961	.38962	1.4×10^{-4}	8.4×10^{-5}	1.0×10^{-4}
87	.39006	.39009	.39008	4.1×10^{-4}	4.2×10^{-4}	4.1×10^{-4}
137	>.4012	.40233	.4025		3.4×10^{-3}	3.2×10^{-3}

(a) Bernstein et al. [6].

(b) Bain and Bardsley [11].

(c) Dickinson [20].

TABLE 2.3

v	J	$E_{nJ}(cm^{-1})$			$\Gamma_{nJ}(cm^{-1})$	
		τ_d(max)	A(max)	BC(Airy)	A(E,J)	JWKB
0	38	7510.0	7514.0	7508.7	98.1	87.0
0	37	6513.3	6513.5	6513.3	5.98	5.60
1	35	5549.8	5550.0	5549.7	14.3	14.9
2	33	4688.4	4689.0	4688.2	20.8	22.5
3	31	3925.0	3925.4	3924.9	25.1	26.7
4	29	3254.7	3255.4	3254.8	25.4	28.4
5	27	2673.0	2673.8	2673.4	25.8	29.3
6	25	2175.0	2176.0	2175.7	27.4	31.4
7	23	1755.3	1756.7	1756.4	31.7	36.9
8	21	1407.0	1409.4	1409.4	42.1	48.3
9	19	1121.6	1127.2	a	66.2	a
9	18	725.9	725.9	726.0	0.53	0.55
10	16	586.0	586.0	586.1	2.93	3.22
11	14	480.1	481.0	481.7	18.5	22.3
11	13	199.4	199.4	199.4	0.005	0.0053
12	12	385.0	398.6	a	11.6	a
12	11	215.5	215.5	215.6	2.62	3.09

TABLE 2.3 (cont'd.)

v	J	$E_{nJ}(cm^{-1})$			$\Gamma_{nJ}(cm^{-1})$	
		τ_d(max)	A(max)	BC(Airy)	A(E,J)	JWKB
13	9	195.0	205.6	a	89.6	a
13	8	89.9	90.0	90.1	1.89	2.38
14	6	81.9	121.0	a	79.0	a
14	5	45.7	49.2	a	26.4	a
14	4	3.76	3.76	3.76	0.007	0.0085

[a] The boundary condition places this level above the barrier maximum.

TABLE 2.4

v	J	$\hbar\bar{\omega}$[a]	$\Gamma^{(0)}$[b]	$\Gamma^{(1)}$[c]	Γ_{exact}[b]	q[d]	t
0	38	1050	87.0	69.8	98.1	.9983	62.5
1	35	1000	14.9	14.2	14.3	.9752	15.2
2	33	950	22.5	21.0	20.8	.9775	13.5
3	31	900	26.7	24.5	25.1	.9778	12.1
4	29	875	28.4	25.8	25.4	.9773	11.1
5	27	800	29.3	26.3	25.8	.9765	9.97
6	25	750	31.4	27.8	27.4	.9767	9.13
7	23	675	36.9	31.7	31.7	.9799	8.44
8	21	600	48.3	39.0	42.1	.9875	8.66
11	14	400	22.3	19.1	18.5	.9608	4.27

[a] Estimates of $\hbar\bar{\omega}$ derived by graphical extrapolation from the tables of LeRoy [40] have been rounded to ±25 cm^{-1}. The level of agreement between $\Gamma^{(1)}$ and Γ_{exact} is unaffected by a change of 100 cm^{-1} in $\hbar\bar{\omega}$.

[b] LeRoy and Bernstein [10].

[c] Equations (2.83).

[d] From energy levels in table 2.3 and V_J^{max} given by LeRoy [50].

TABLE 3.1

	State	Type	$E - E_x$ (cm^{-1})	ΔF (cm^{-1} $\AA^{-1}$)	R ($\AA$)	Range ($\AA$)	References
O_2	$B^3\Sigma_u^-$	c^+	5000	50,000	1.89	±0.10	[56, 65]
I_2	$B^3\pi(O_u^+)$	c^-	3000	9,000	2.87	±0.15	[63, 68]
OH	$A^2\Sigma^+$	c^+	4000	24,000	1.65	±0.20	[61, 67]

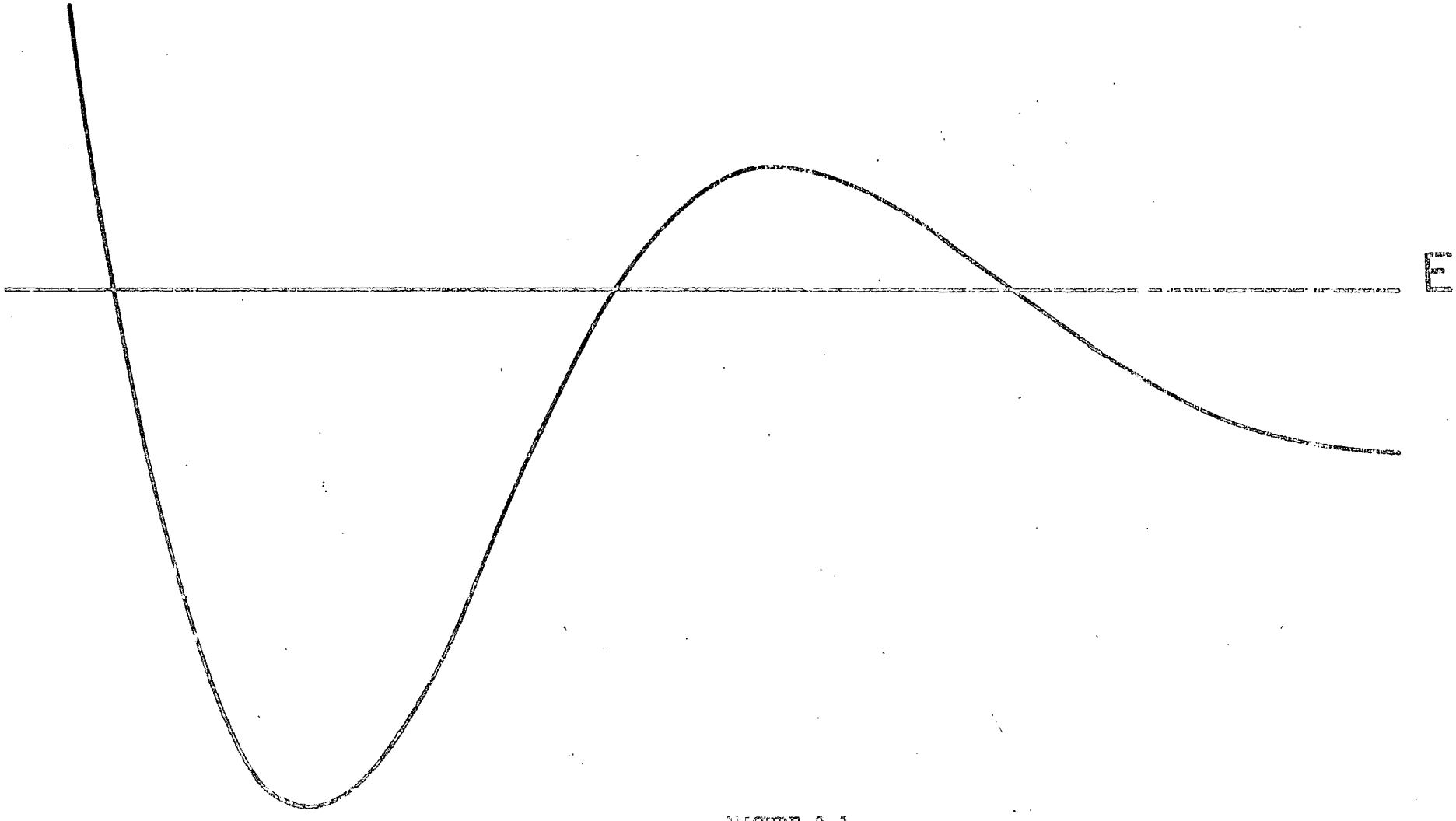

FIGURE 2.1

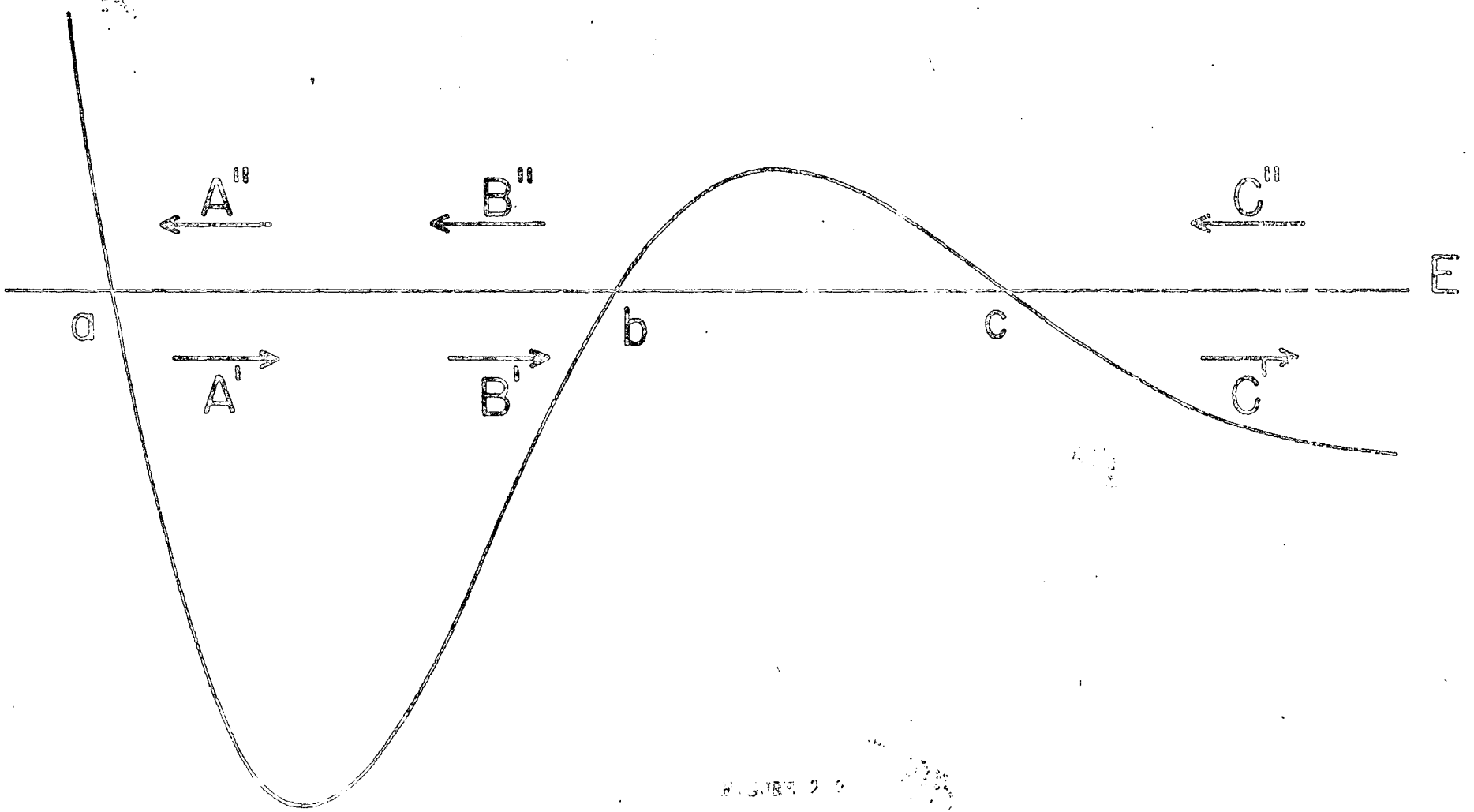

FIGURE 2.9

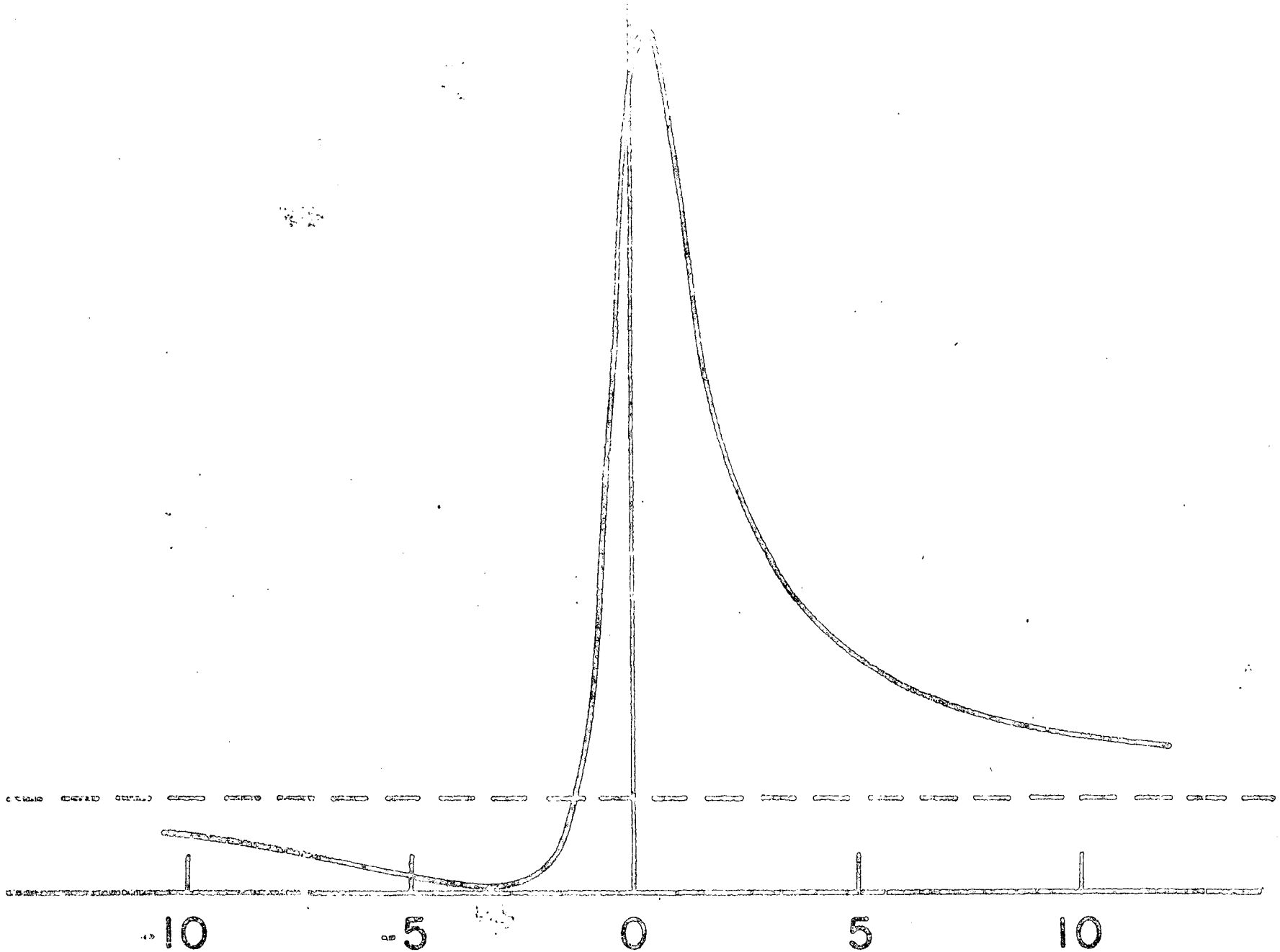

FIGURE 3.1

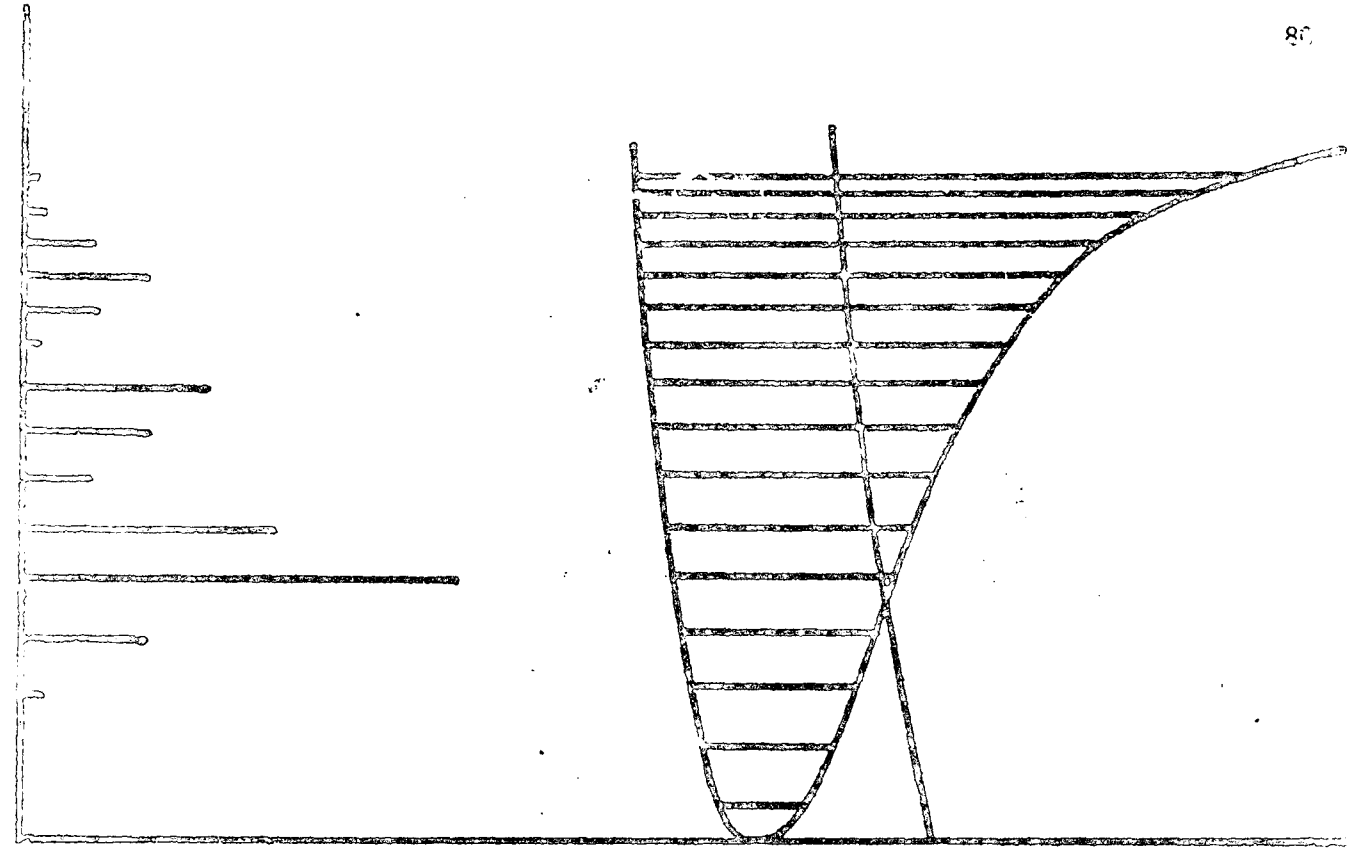

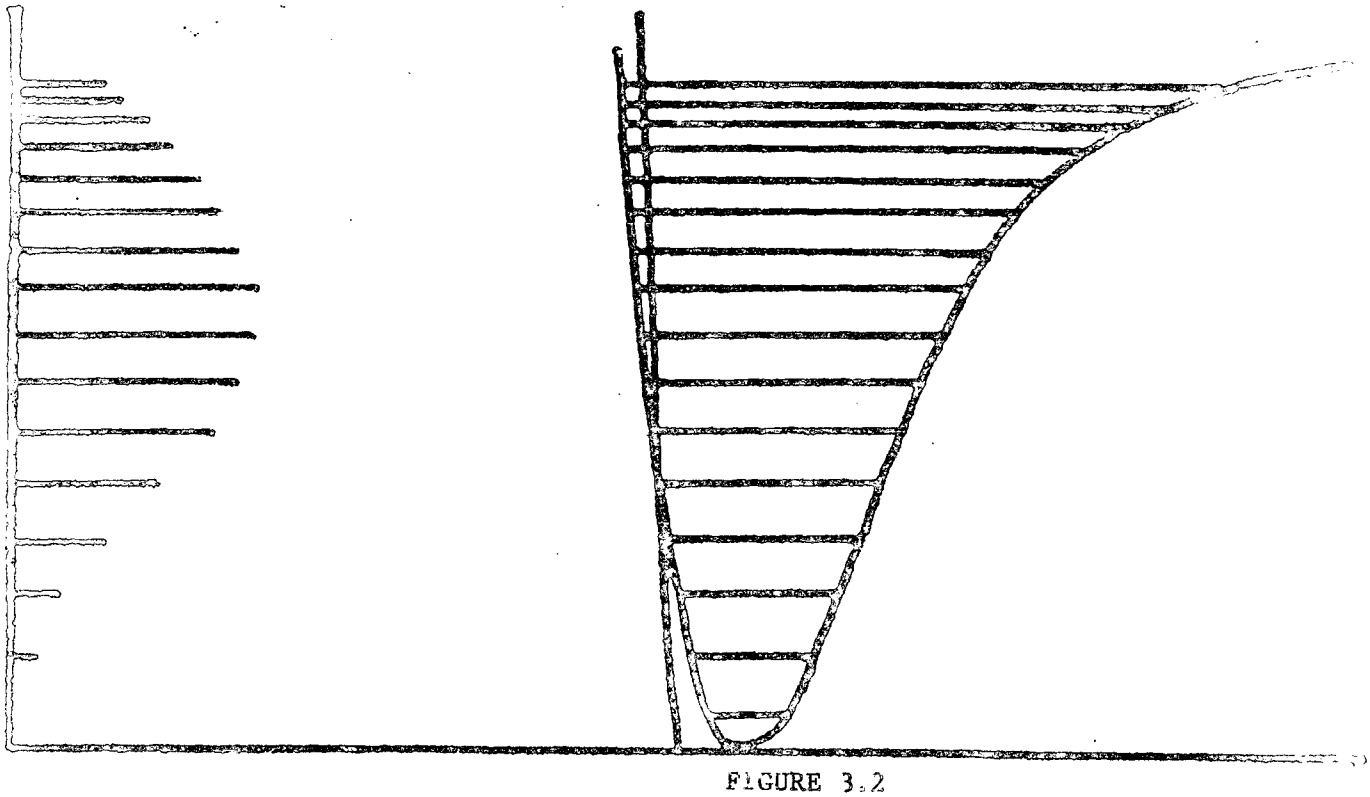

FIGURE 3.2

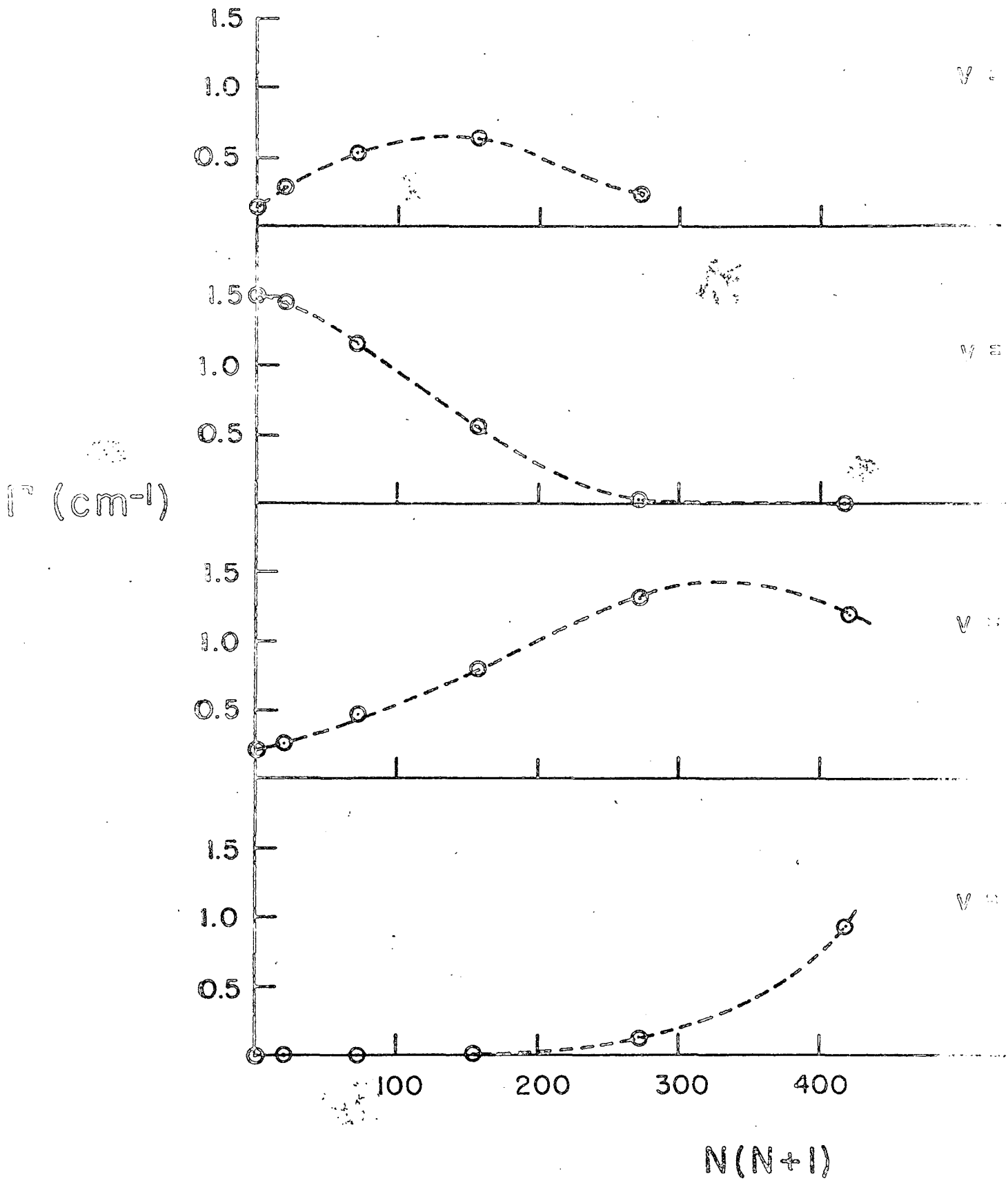

FIGURE 3.3

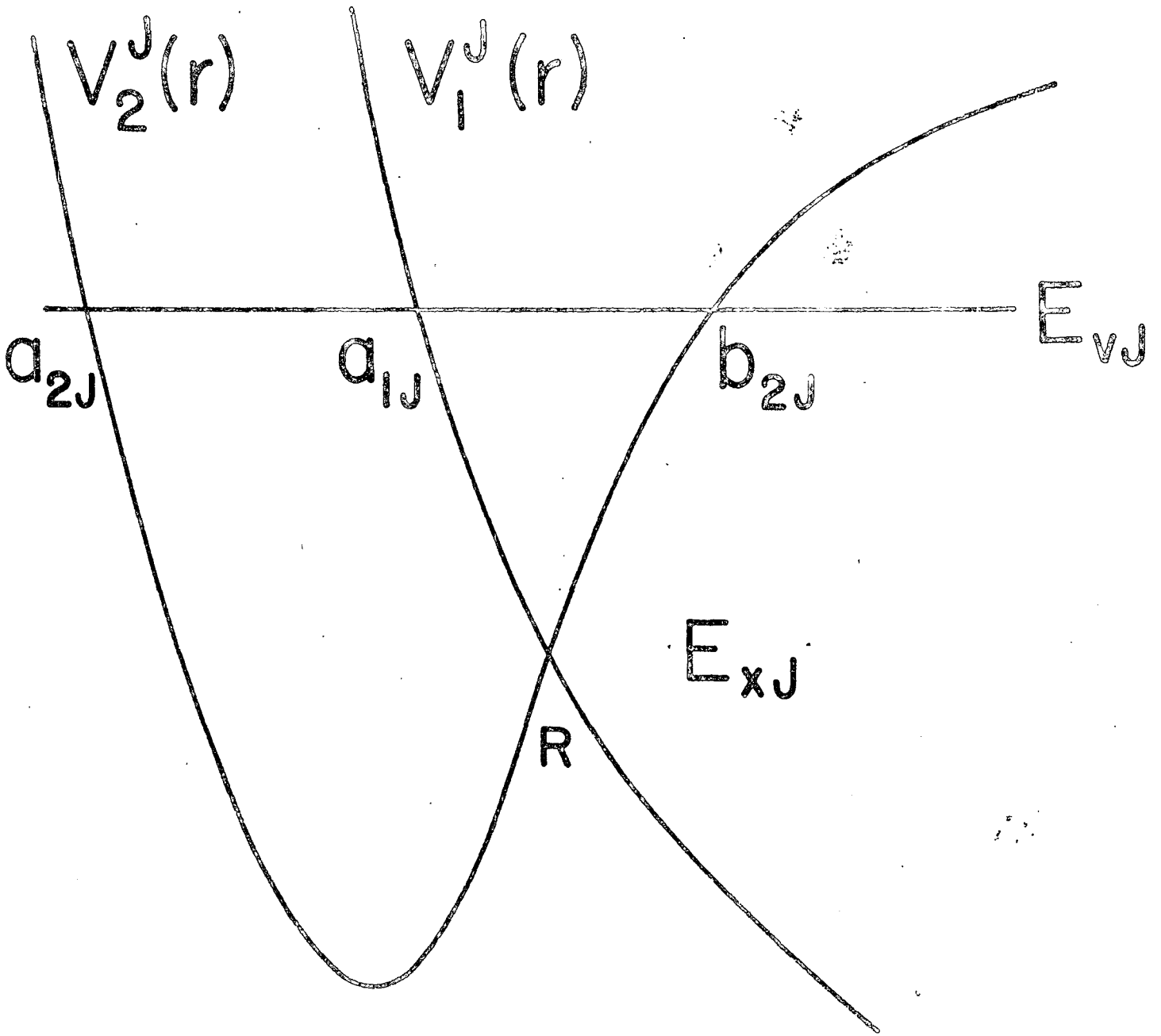
$V_2^J(r)$
$V_1^J(r)$
E_{vJ}
a_{2J}
a_{1J}
b_{2J}
E_{xJ}
R

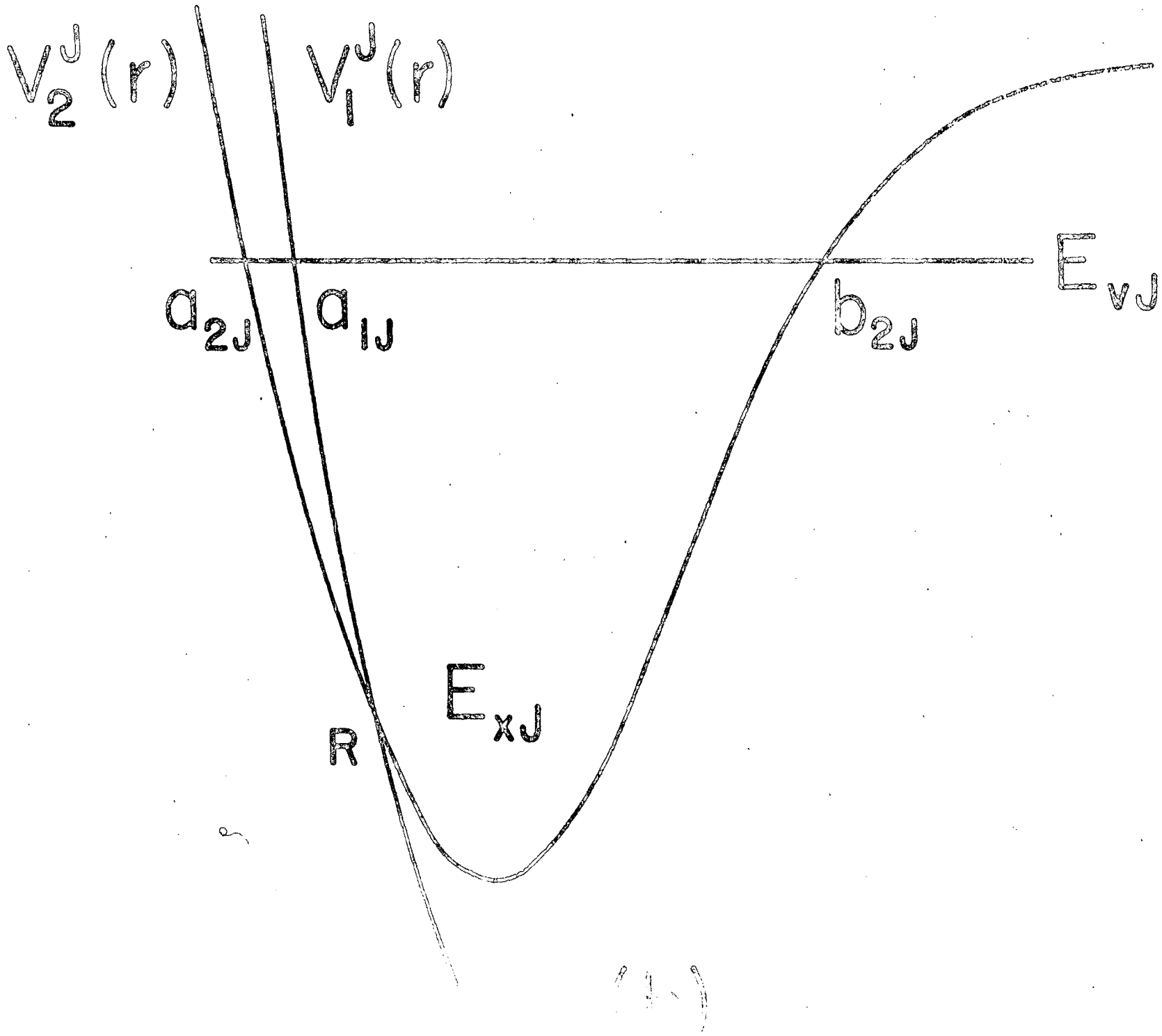
$V_2^J(r)$
$V_1^J(r)$
E_{vJ}
a_{2J}
a_{1J}
b_{2J}
E_{xJ}
R

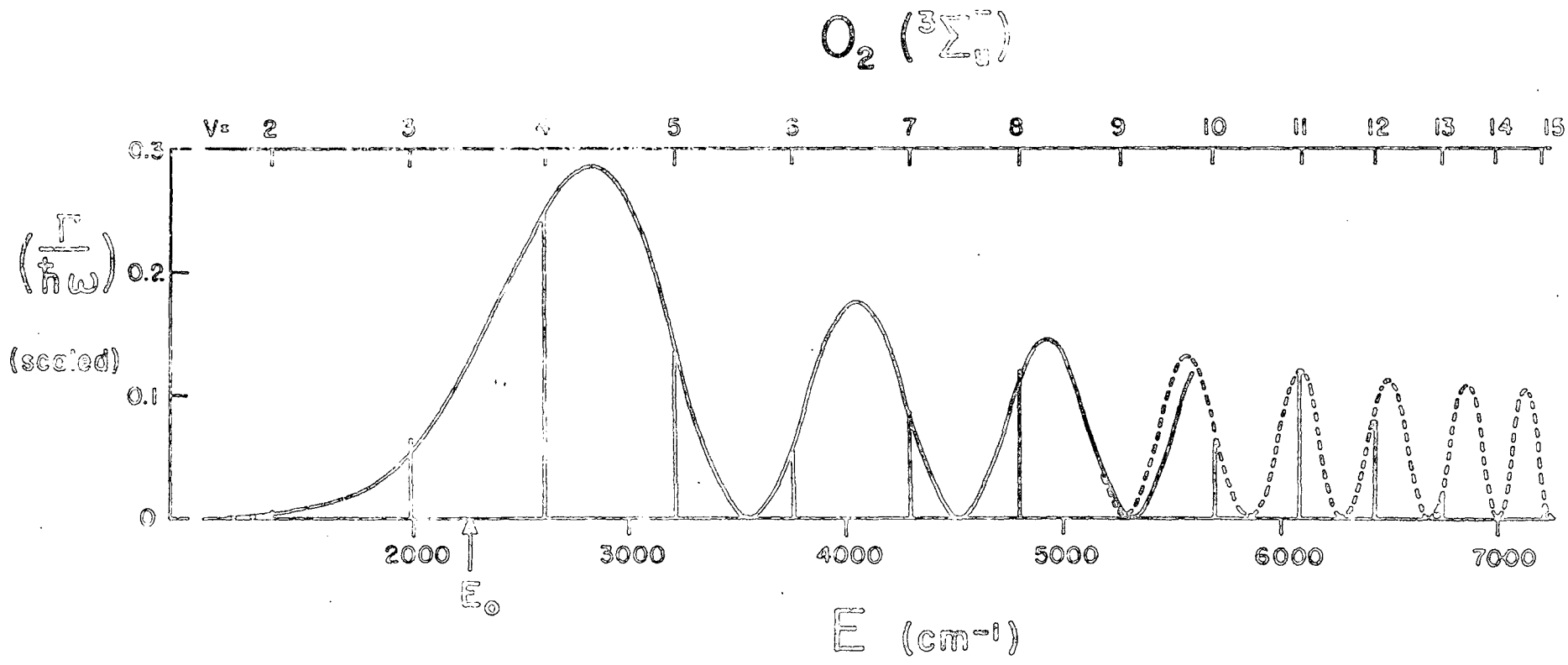
O_2 ($^3\Sigma_g^-$)
V_a 2 3 4 5 6 7 8 9 10 11 12 13 14 15
0.3
0.2
0.1
0
$\left(\frac{\Gamma}{\hbar\omega}\right)$
(scaled)
2000
3000
4000
5000
6000
7000
$E_\odot$
E (cm^{-1})

F 2037 3.5

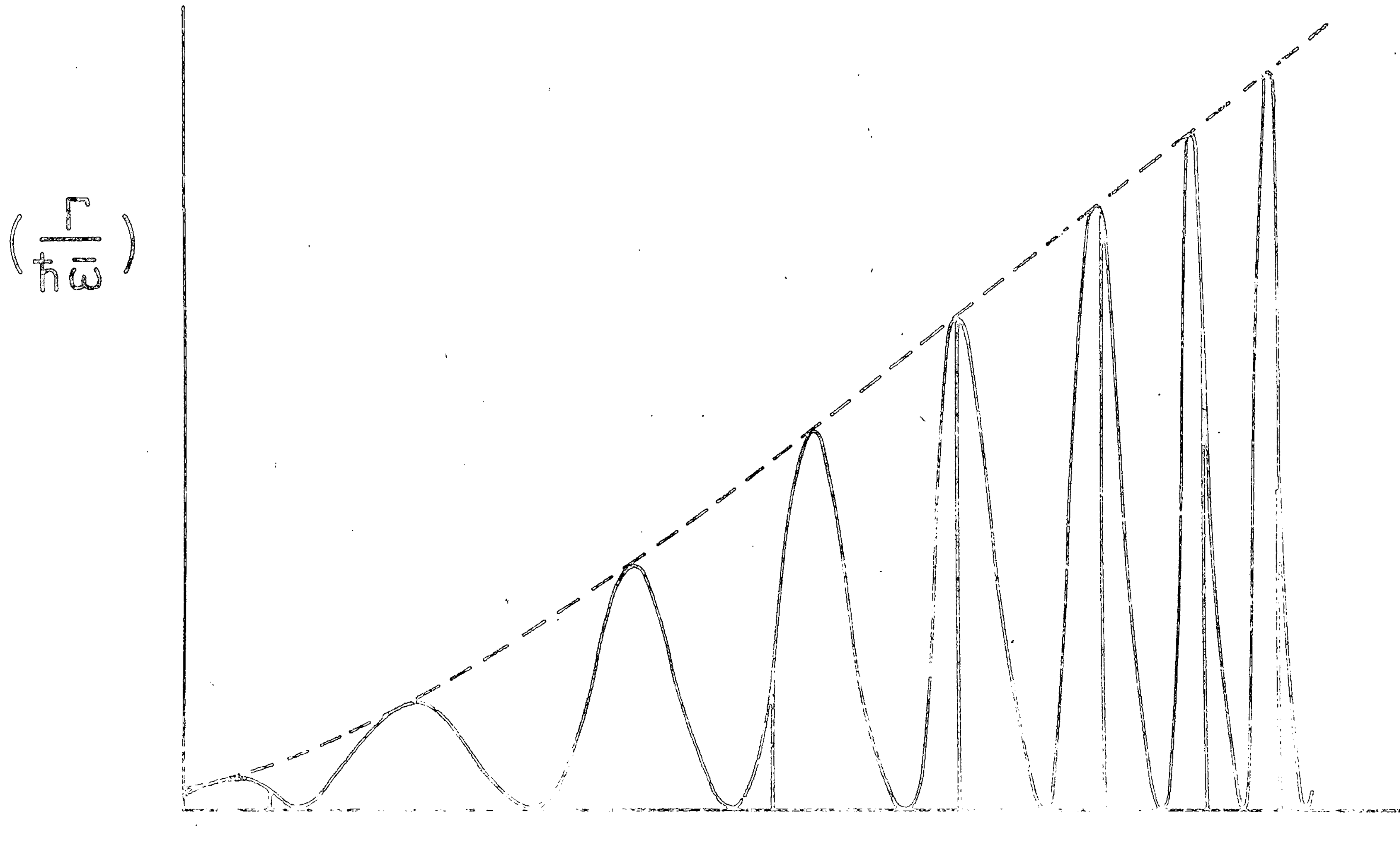

$\left(\frac{\Gamma}{\hbar\bar{\omega}}\right)$

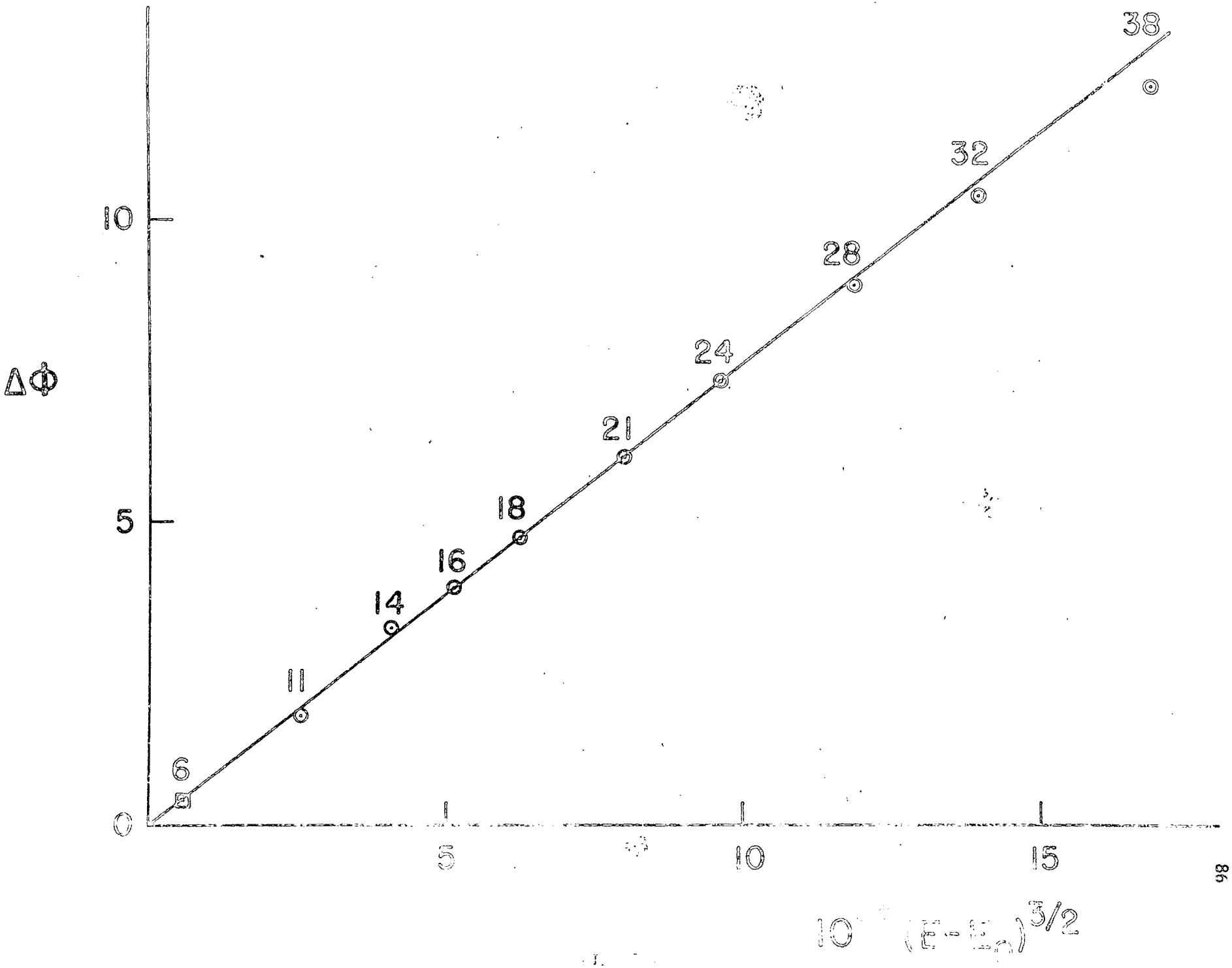
38
32
28
24
21
18
16
14
11
6
10
5
0
ΔΦ
5
10
15
$10^{-3}(E-E_0)^{3/2}$

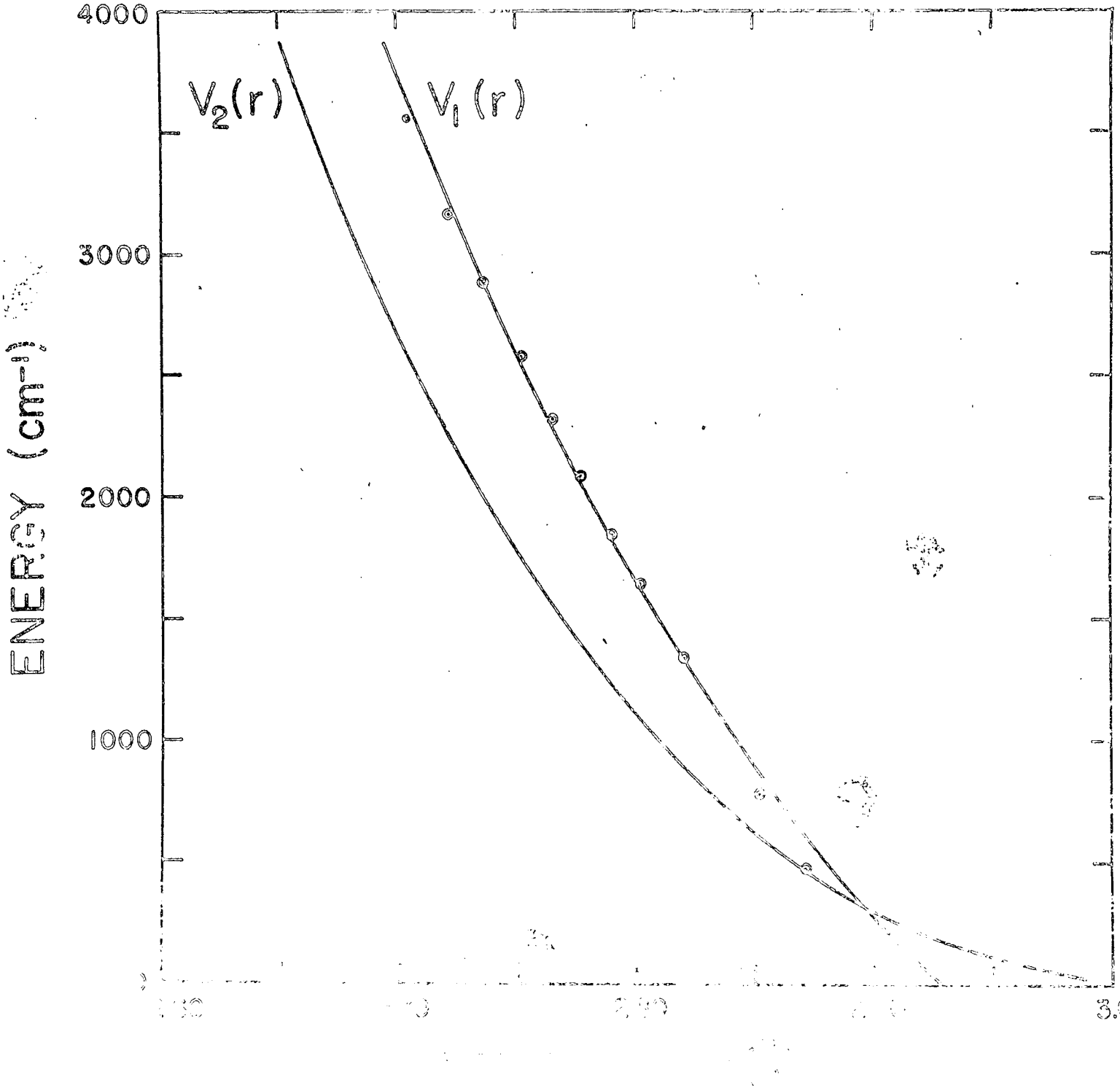
4000
3000
2000
1000
ENERGY (cm⁻¹)
V₂(r)
V₁(r)
3.0